Multiple Linker Screening Strategies for the Development of New Microporous Coordination Polymers with Remarkable Surface Area

Jacob Van Oosterhout

Submitted as a requirement for graduation from the University of Michigan

Acknowledgments

First of all, I would like to thank Professor Adam Matzger for being an extremely knowledgeable and helpful mentor, for having the trust in me to allow me a degree of autonomy, and for fostering a unique and challenging research environment. I am also deeply indebted to the University of Michigan and specifically UROP for providing me with the opportunity to perform undergraduate research in a world-class environment. I would like to thank Jennifer Schnobrich and Kyoungmoo Koh, with whom I closely collaborated with, for their careful guidance and eagerness to provide pointers and to challenge my assumptions until every statement could be backed up with robust data. The entire Matzger group deserves acknowledgement for their friendliness and eagerness to help out an undergrad, and I would like to especially thank Jeremy Feldblyum for his collaboration in exploring the properties of a particularly tricky MCP, and Antek Wong-Foy for his assistance with the technical equipment the research required.

I would be nothing (literally) without my family, and would like to thank my father Bob, my mother Mary Ann, and my sister Maika for bearing my twenty-two years with grace and poise. I would like to thank my father for teaching me how to ask questions, and for managing my stress when experiments invariably performed poorly. Last, but certainly not least, I would like to thank my great-uncle, Howard Burke, for fostering in me a love of chemistry and for inspiring me to continue the "family tradition" of chemistry research. His experiences gave me a direction to point towards during my tumultuous early undergraduate years. For that, and to honor a long and productive career of organic research, I dedicate this thesis to Howard Burke.

Table of Contents

Chapter 1 - Introduction to Synthesis of Microporous Coordination Polymers

1.1 Introduction

Microporous coordinating polymers (MCPs) are composed of metal ions or metal clusters joined by organic ligands, also called linkers, which can produce a rigid, microporous, crystalline framework based on the flexibility of the organic linker. Research concerning MCPs has exploded in the recent past due to enticing features such as ultra-high surface area[1] and structural stability, but also due to potential commercial applications in gas storage[2], catalysis[3], and separations of gases[4] and liquids.[5] Variations in linker geometry and the chemical properties of metals enable a sizable array of both established and potential avenues for MCP formation.

1.2 General Concepts

Reticular Synthesis

The vast array of avenues for MCP formation can render MCP discovery more of an art than a science. Logical methods to predict how separate building units will combine to form an MCP has been defined as reticular synthesis.[6] Unlike synthetic methodologies prevalent in other fields, such as retrosynthetic analysis in organic synthesis, the structural characteristics of metal clusters and linking ligands are unchanged after reaction. As a result, reticular synthesis uses the chemistry of metal clusters and linkers to predict MCP products. The zinc acetate cluster $[Zn_4O(CO_2)_6]$, for instance, forms an octahedral building unit which, if the carboxylate C-atoms are joined linearly such as with a benzene ring, can form a cubic MCP with high porosity, called MOF-5.[7] Changing the geometry of the organic linker to a triangular unit results in an MCP of a completely different structure with large, well defined pores, known as MOF-177.[8] Dicopper complexes when bonded with carboxylates produce building units utilizing the well-known copper paddlewheel geometric motif. Three carboxylates joined by a benzene ring in the form of

benzene-1,3,5-tricarboxylic acid form another stable MCP, HKUST-1.[9] Combining the chemistry of metal clusters with the geometry of linking ligands enables prediction and discovery of a vast array of MCPs.

Surface Area and the BET Method

Adsorption refers to the process in which gas molecules come into contact with a solid and, due to intermolecular forces, accumulate next to the adsorbant.[10] The ability of MCPs to adsorb gases is the most widely studies and potentially valuable aspect of MCP chemistry. Since MCPs are composed of repeating units of porous frameworks, an MCP crystal has a vast quantity of accessible pores, and accordingly, a large surface area for gas molecules to adsorb. Adsorption information of MCPs is obtained by measuring gas uptake at a constant temperature. Two primary models exist to correlate gas adsorption with accessible surface area. The Langmuir model assumes that gases adsorb in monolayers directly to the walls of the adsorbant. An alternative model proposed by Brunauer, Emmet and Teller, called the BET model, assumes multiple layers are able to accumulate on the adsorbant, a process known as multilayer adsorption.[11] The possibility of multilayer adsorption results in the Langmuir model tending to overestimate the accessible surface area of an MCP, rendering the BET model the preferred predictive tool. Adsorption analysis in this thesis will use the BET model to predict surface areas.

Interpenetration

Interpenetration is defined as the nonchemical conjoining of two separate frameworks in such a fashion that separation of the frameworks would require the breaking of multiple bonds.[12] Interpenetration greatly decreases the accessible pore size of a given MCP and consequently reduces the accessible surface area. Two frameworks can either interpenetrate such that the

distance between the two lattices is maximized, which interpenetration specifically refers to, or such that the distance between the two lattices are minimized, which is referred to as catenation. Interpenetrated frameworks, despite significantly lower surface area, can still maintain significant porosity[13] sufficient to selectively adsorb gases. The studies contained in this thesis primarily focus on maximizing accessible surface area of MCPs, so the differences between interpenetrated and catenated structures are not relevant for the purposes of these studies.

Methodologies for MCP Characterization

X-ray diffraction is the most powerful tool available to chemists who wish to know the precise structure of a crystalline solid. Two primary types of x-ray diffraction exist: single-crystal x-ray diffraction and powder x-ray diffraction (PXRD). Single-crystal x-ray diffraction shines an intense x-ray beam upon a crystal sample with minimal imperfections. X-rays are diffracted by atoms in the crystal onto an x-ray detector. Analysis of the diffraction patterns can produce a solved crystal structure. Single-crystal XRD is time consuming and requires very careful growth of MCPs. PXRD, alternatively, uses powdered crystalline samples to yield a pattern which is unique to the crystal's unit cell. PXRD cannot directly be used to solve the unit cell of a crystal, but the unit cell can be modeled using various programs. Predicted powder patterns can easily be obtained from these models and compared to experimental powder patterns.

1.3 Strategies Employed in MCP Discovery

Reticular synthesis remains a widely used strategy for MCP discovery. A specific offshoot of reticular synthesis uses linkers which are similar to other linkers known to combine with metal building units to yield MCPs, a process known as isoreticular anaylsis. Isoreticular synthesis was coined by Yaghi, et al. in 2002 to yield the isoreticular metal-organic framework (IRMOF) series of cubic MCPs.[14] The IRMOF series of MCPs expanded on the MCP morphology known

to arise from a mixture of linear terephthalic acid linkers with Zn_4O clusters to yield cubic MOF-5. Variation of the geometry of linear linkers yielded cubic MCPs. Similar isoreticular studies were also applied to triangular tritopic linkers of increasing size and copper salts to yield MCPs of increasing porosity.[15] Isoreticular studies come at a cost, since increasing linker size also increases the likelihood of interpenetration while decreasing the structural stability of the MCP. If an MCP encompases too much open space and thus lacks structural integrity, its structure may collapse upon removal of solvent from crystal pores. Alternate methods for discovery of MCPs involve examining unique linker geometries to formulate different building units for MCP growth.

1.4 Research in the Matzger Group

The Matzger group has probed the cutting edge of MCP chemistry for the better part of a decade, and has employed various methodologies for MCP discovery. Research in the Matzger group demonstrated the ability to form MCPs from asymmetric linkers,[16] developed a theoretical platform for predicting an MCP's surface area based upon the ratio between the atomic mass of the linker and metal,[17] and pioneered polymer-induced heteronucleation as a method to synthesize MCPs with different structures than MCPs that are obtained under more traditional methods.[18]

UMCM-1 and UMCM-2, two MCPs displaying exceptionally high surface areas, were among the first MCPs to show the value of mixed-linker systems in the synthesis of highly porous MCPs.[19,20] UMCM-1 combined a linear ditopic linker and a triangular tritopic linker with Zn_4O clusters to yield an MCP with very large pores. Lengthening the linear linker slightly yielded UMCM-2, an MCP with a then-record BET surface area. UMCM-1 and UMCM-2 demonstrated the ability to synthesize MCPs with surface areas in excess of the highest surface areas obtained

from MCPs composed of just one linker while also avoiding interpenetration and other structural defects.

In addition, the Matzger group demonstrated a mixture of two linear linkers based on 4,4'-biphenyldicarboxylic acid (H_2BPDC) with constituent groups on the benzene rings form cubic MCPs with greatly reduced interpenetration in comparison with MCPs formed from linear unsubstituted linkers.[21] Reaction of (H_2BPDC) with $Zn(NO_3)_2$ yields a doubly interpenetrated IRMOF-9 or, under extremely specific conditions not viable for industrial scale, non-interpenetrated IRMOF-10.[22] Interpenetrated IRMOF-9 has a BET surface area of 1700 m^2/g, while noninterpenetrated IRMOF-10 has a theoretical BET surface area of approx. 5000 m^2/g.[23] Replacement of H_2BPDC with 2,2',6,6'-tetramethylbiphenyl-4,4'-dicarboxylic acid (H_2Me_4BPDC) added some steric bulk to the linker, but the steric hindrance provided by four methyl groups was insufficient to prevent interpenetration. Replacement of H_2BPDC with the extremely bulky 9,10-bis(triisopropylsilyloxy)phenanthrene-2,7-dicarboxylate (TPDC, Figure 1.1) was sufficiently bulky to inhibit interpenetration but also blocked adsorption sites. A mixture of H_2Me_4BPDC and TPDC with $Zn(NO_3)_2$ was found to yield a MCP with surface area of up to 3000 m^2/g. The results demonstrated that strategies exist to use a system of mixed linkers of similar geometry to inhibit interpenetration while still yielding high surface areas.

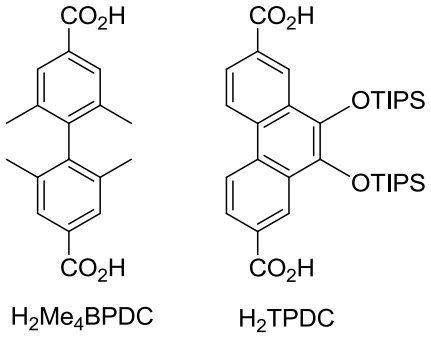

Figure 1.1. H_2Me_4BPDC and H_2TPDC.

1.5 Content of Thesis

The contents of the thesis described below examine the viability of using two linear linkers of different lengths to afford highly porous MCPs while avoiding interpenetrated structures. Research in the Matzger lab has demonstrated the viability of mixed linker systems in which the linkers are of different geometry. Linkers of similar geometry but with different steric-hindering groups can be combined to produce non-interpenetrated MCPs as well. This thesis displays the viability of an alternate strategy for MCP design. Instead of adding different bulky groups to yield a randomly mixed MCP, a mixture of two linear linkers of different length can yield highly structured, highly stable MCPs with high surface area which are not prone to interpenetration. Chapter two presents the synthesis of a UMCM-8, an MCP composed of two linear linkers possessing remarkable surface area with no evidence of interpenetration. Chapter three presents an isoreticular study based upon the results of the previous chapter, and shows the synthesis of UMCM-9, an isostructural MCP to UMCM-8 with a BET surface area of almost 5000 m^2/g. In addition, a screen composed of three separate linear linkers of different lengths is shown and analyzed. The results contained herein demonstrate the viability of systems of mixed linear linkers to afford highly porous MCPs, which opens the sizable library of linear linkers to be studied for viable 2-linker combinations.

Chapter 2 - Development of an MCP with remarkable surface area from mixture of two linear linkers

2.1 Introduction

The discovery and synthesis of new MCPs with desirable properties tends to focus on the reaction between an organic linking ligand and a metal cluster. Many researchers require a great deal of trial and error to discover conditions which yield MCPs with large BET surface areas. Reticular chemistry, or the examination of the geometry of the linker and metal ion used, can predict the structure of an MCP. For example, Yaghi, et al, demonstrated with the IRMOF-X series that linear linkers combine with octahedral Zn_4O clusters to yield cubic MCPs with high porosity. MOF-5, the simplest MCP of the IRMOF-X series, is composed of 1,4-benzenedicarboxylic acid and Zn_4O clusters. MOF-5 has a very good BET surface area of 3362 m^2/g.[24] Current models predict an MCP isostructural to MOF-5 but with longer linkers to have a greater BET surface area.[17] However, IRMOF-8, a cubic MCP composed of Zn_4O clusters and 2,6-napthalenedicarboxylic acid (H_2NDC) can only reach a BET surface area of 1466 m^2/g, which is much lower than the maximum available BET surface area derived from the crystal structure (4390 m^2/g).[17] The severely reduced accessible surface area occurs due to interpenetration of IRMOF-8 lattices. The overlapping crystal lattices impede gas adsorption and reduce the effective surface area of an MCP.

2.2 Two-Linker Syntheses of Highly Porous MCPs

When multiple linkers are combined in the same pot in the presence of metal ions, one of two reactions can occur. Each linker can react independently with the metal cluster different MCPs composed of only one linker species, a process known as segregation. The linkers can also combine together to produce a new material in a process known as copolymerization. Literature data suggests that multiple linkers can induce copolymerization to yield MCPs with very high

surface areas. In our group, Kyoungmoo Koh presented the synthesis of UMCM-1 (University of Michigan Crystalline Material), a highly porous MCP produced from H_3BTB, 1,4-benzinedicarboxilic acid (H_2BDC) and zinc nitrate hexahydrate. UMCM-1 possesses a very high BET surface area of 4160 m^2/g. BDC and BTB copolymerized to form UMCM-1 only between mole ratios of 3:2 and 1:1 BDC:BTB, and in other cases yielded a mixture of MOF-5, MOF-177, and UMCM-1 (Figure 2.1).

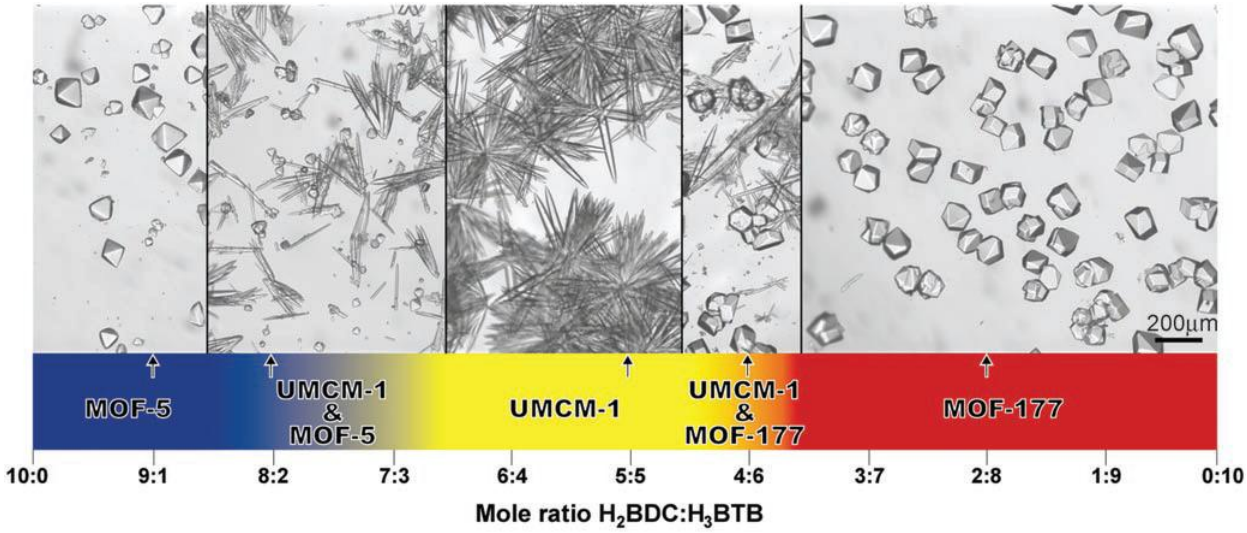

Figure 2.1. Different phases resulting from reacting different mole ratios of BDC and NDC.[19]

2.3 Strategy

Octahedral Zn_4O clusters and linear H_2BDC and H_2NDC linkers can be arranged to form a specific number of tetragonal or cubic cages (Figure 2.2). We predicted

an MCP composed of both cubic and tetragonal cages would reduce interpenetration while maintaining a robust, stable structure.

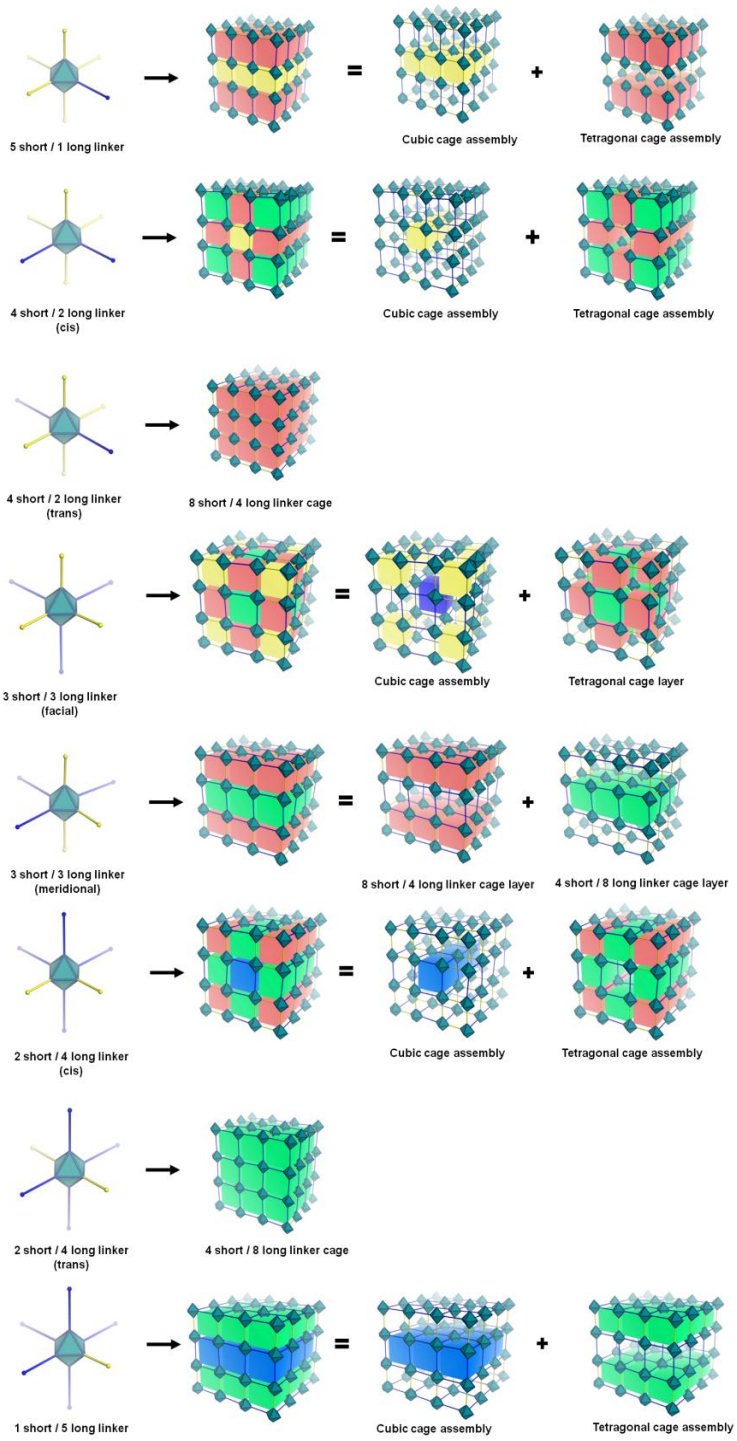

Figure 2.2. Possible cubic and tetragonal cage structures resulting from different arrangements of long and short linear linkers with octahedral metal clusters.

A 2-linker screen composed of H_2BDC and H_2NDC would allow in depth study of the differing structures which can result from a mixture of linear linkers. The screen would enable an

understanding of which long/short linker combinations would segregate and which combinations would copolymerize into one of the cubic or tetragonal cage structures in Figure 2.2. In addition, we would be able to discern whether or not one linker arrangement predominates over the others. Mixed-linker solutions run the risk of having small quantities of segregated MCPs growing on a copolymerized MCP, which would pose problems for single crystal x-ray diffraction. In order to accurately determine the unit cell, a crystal sample must be pure and free of irregularities. Since all possible structures which may result from the screen are known, the unit cells can be modeled using Materials Studio. Predicted powder x-ray diffraction patterns can then be compared to experimental powder x-ray diffraction patterns to determine crystal structure.

2.4 Analysis of BDC-NDC screen

A screen of base-ten mole ratios of H_2BDC and H_2NDC dissolved in diethylformamide (DEF) with Zn_4O clusters obtained isolated a pure MCP with a PXRD pattern different from existing MCPs, [25] which we called UMCM-8 at a 1:1 mole ratio of BDC to NDC (Figure 2.3). Pure MOF-5 was observed in all samples with a mole ratio of BDC:NDC of 7 or greater. A 6:4 mole ratio of BDC:NDC yielded a mixture of UMCM-8 and MOF-5.

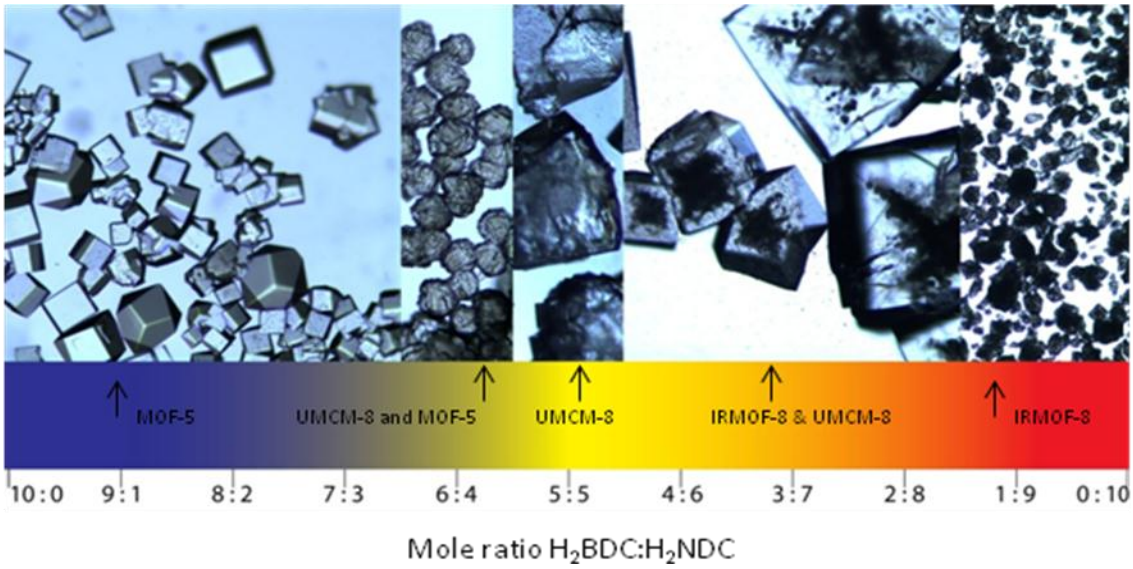

Figure 2.3. MCPs obtained from various mol ratios of H_2BDC and H_2NDC.

Samples containing between 60 and 80 mol % NDC were observed to have cubic UMCM-8 growing around impure phase crystals appeared similar to the highly phase-impure IRMOF-8 obtained in DEF. As a result, we hypothesize that IRMOF-8 forms more readily than UMCM-8 in samples of 40 mol % BDC or less and thus serves as a nucleation point for UMCM-8 growth. MCPs have been demonstrated to be able to form core-shell MCPs, where previously formed MCP grows a shell composed of a different MCP.[26] Previous syntheses of core-shell MCPs required seed MCPs to be obtained in one sample, which is then replaced with new mother liquor containing the requisite linkers and metal clusters for formation of the shell MCP. A mixture of H_2BDC and H_2NDC in mole ratios of 40% BDC or less appears to exhibit one-pot core-shell MCP growth. However, the IRMOF-8 obtained from DEF is very phase-impure, and more rigorous studies than visual observation to prove one-pot core-shell UMCM-8 and IRMOF-8 growth would be very difficult to perform.

^{1}H-NMR analysis of the BDC-NDC screen shows the mol % BDC increasing in obtained samples as the mol % BDC increased in solution preparation.[27] Initial samples with 70 mol % or

greater BDC content yielded samples with zero observed NDC, representing pure MOF-5 (Figure 2.4). A 1:1 mol ratio of BDC:NDC produced UMCM-8 composed of 45% BDC.

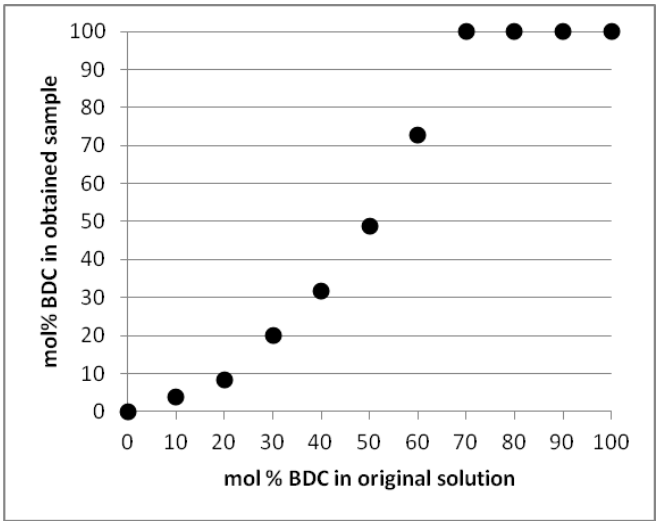

Figure 2.4. Mol % BDC obtained by using various ratios of BDC and NDC in the presence of zinc nitrate.

The mol % in obtained samples closely matches a quadratic polynomial function when plotted against mol % BDC in original solution. This correlation supports the hypothesis that quickly forming IRMOF-8 serves as a nucleation point for UMCM-8. Formation of IRMOF-8 would remove an excess of NDC from solution, which leaves less NDC to copolymerize with BDC to form UMCM-8. MOF-5 appears not to engage in one-pot core-shell formation since unreacted BDC is lost upon removal of mother liquor. Since 1:1 mol ratio of BDC:NDC yields a sample of 45 mol% BDC, we suspect slight quantities of IRMOF-8 exist in the center of UMCM-8 crystals. The IRMOF-8 in the UMCM-8 crystals can disrupt attempts to solve the structure via single-crystal x-ray diffraction while not having an overly adverse effect on surface area.

BDC quantities greater than 50 mol % showed that excess BDC overwhelmingly favored MOF-5 formation. Without a similar quantity of NDC, BDC will bind only to zinc clusters bound to other BDC molecules to form MOF-5. Mechanistic studies, in which a mixture of BDC and NDC is dissolved in deuterated n,n'-diethylformamide (DEF), and aliquots of mother liquor are

analyzed via NMR at specific intervals could give insights towards the rates of formation of IRMOF-8 and UMCM-8, but such studies would have significant drawbacks and difficulties, not the least of which is the fact that deuterated DEF is not commercially available.

Optimal surface area was obtained when the crystals had 45 mol % BDC. As the quantity of BDC increased from 45 mol %, the surface area decreased to that of MOF-5. The surface area decreased to that of IRMOF-8 as the quantity of BDC decreased from 45 mol %. No other trends are apparent from the data (Figure 2.5).

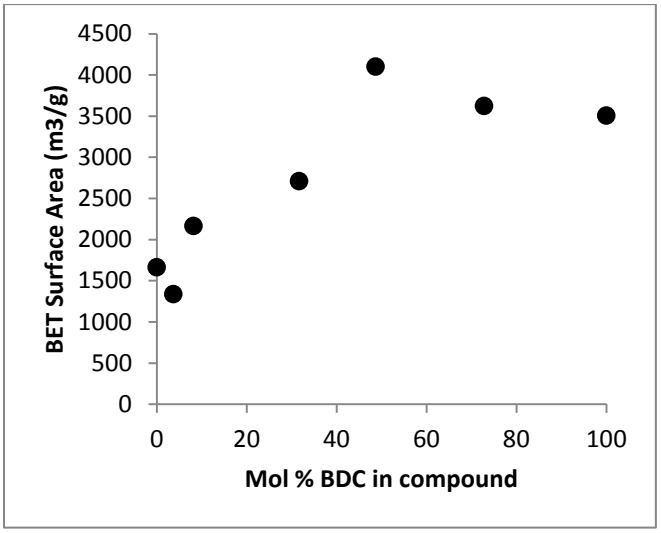

Figure 2.5. BET surface areas of samples prepared from various ratios of BDC and NDC in the presence of zinc nitrate.

2.5 Characterization of UMCM-8

Single crystal x-ray diffraction of UMCM-8 obtained from a 1:1 BDC:NDC mol ratio in diethylformamide (DEF) failed to solve the crystal structure. Single crystal x-ray diffraction requires a pure single crystal, and could have been disrupted by either other MCPs serving s nucleation points as described above, or by having small quantities of segregated MCPs growing on the MCP surface. Since all possible structures which may result from the screen are known, the unit cells were modeled using Materials Studio. The obtained PXRD pattern of UMCM-8 was compared to a Pawley refinement of simulated powder patterns of the MCPs resulting from

various combinations of BDC and NDC. The experimental powder pattern matched the simulated powder pattern of the MCP composed of 3 BDC and 3 NDC arranged facially (Figure 2.6).

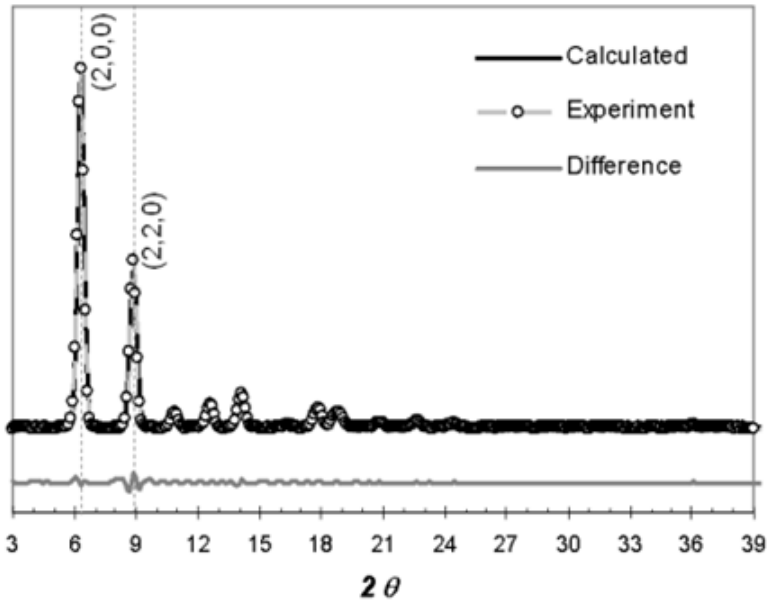

2.6. Overlay of Pawley refinement results from PXRD patterns of simulated fac-$(Zn_4O)(BDC)_3(NDC)_3$and experimental PXRD patterns of UMCM-8.

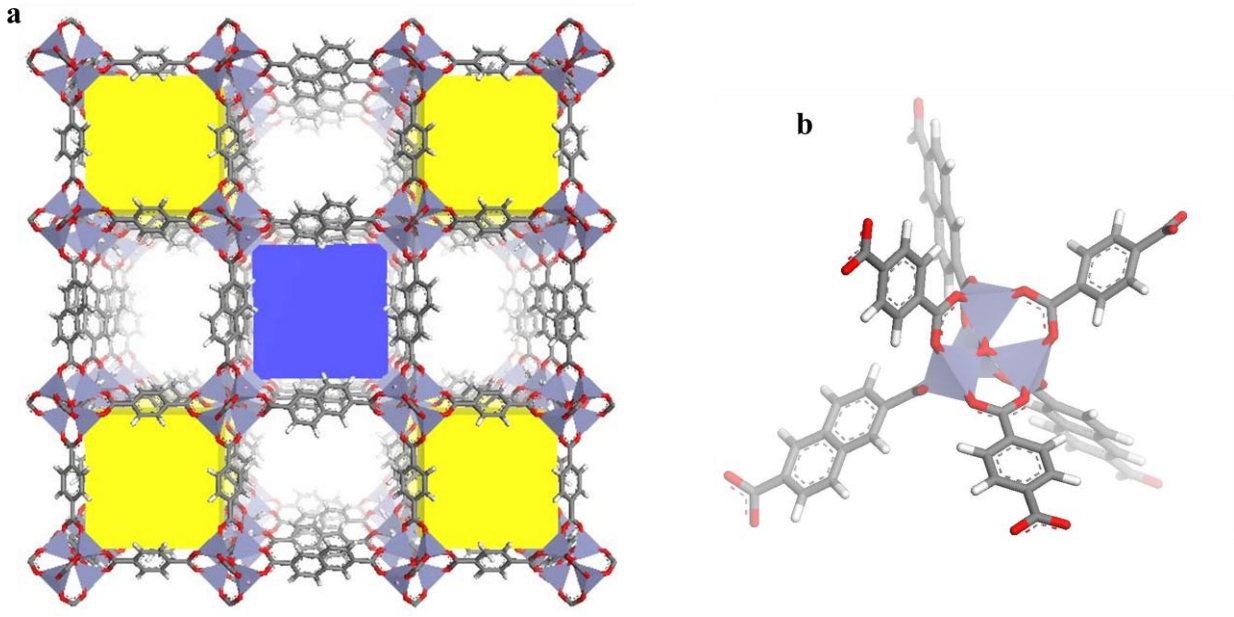

Figure 2.7. a. UMCM-8 unit cell, composed of a cubic NDC and BDC cages connected by the corners. b. Facially arranged $Zn_4O(BDC)_3(NDC)_3$ UMCM-8 clusters.

The unit cell of UMCM-8 is a tetragonal unit cell composed of one cubic BDC cage, 8 cubic NDC cages, 6 tetragonal cages composed of 8 BDC and 4 NDC, and 8 tetragonal cages composed of 4 BDC and 8 NDC.

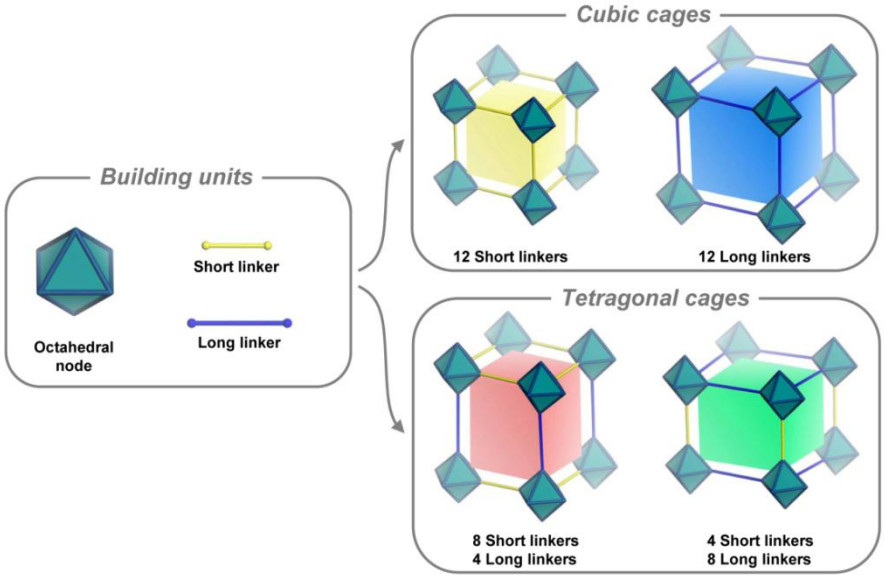

Figure 2.8. Tetragonal cages which compose UMCM-8. Short linkers represent BDC, long linkers represent NDC.

The modeled structure of UMCM-8 predicted a BET surface area of 4005 m^2/g, which is significantly greater than that of both IRMOF-8 and MOF-5.[28] Nitrogen adsorption analysis of UMCM-8 gave a BET surface area of 4030 m^2/g,[29] which translates well to the predicted surface area. The close relationship between predicted and experimental surface areas suggests a lack of structural defects, structural collapse, or interpenetration. BDC cages in UMCM-8's unit cell prevent the BET surface area from exceeding the maximum surface area of non-interpenetrated IRMOF-8. However, the additional complexity of the unit cell effectively inhibits interpenetration of structures.

Thermal gravimetric analysis of UMCM-8 showed two primary weight-loss steps (Figure 2.9). One weight-loss step between 25-100 °C was a 25% weight loss and corresponded to evaporation of CH_2Cl_2 solvent. The second weight-loss step was between 425-525 °C and lost

32% weight, corresponding to structural collapse of UMCM-8. No weight loss steps between the initial solvent evaporation and structural collapse were observed. The pores of UMCM-8 were not too small to prevent the complete evaporation of dichloromethane solvent. The structural collapse weight-loss step shows UMCM-8 to be stable to above 400 °C, displaying similar stability properties to MOF-5.[30]

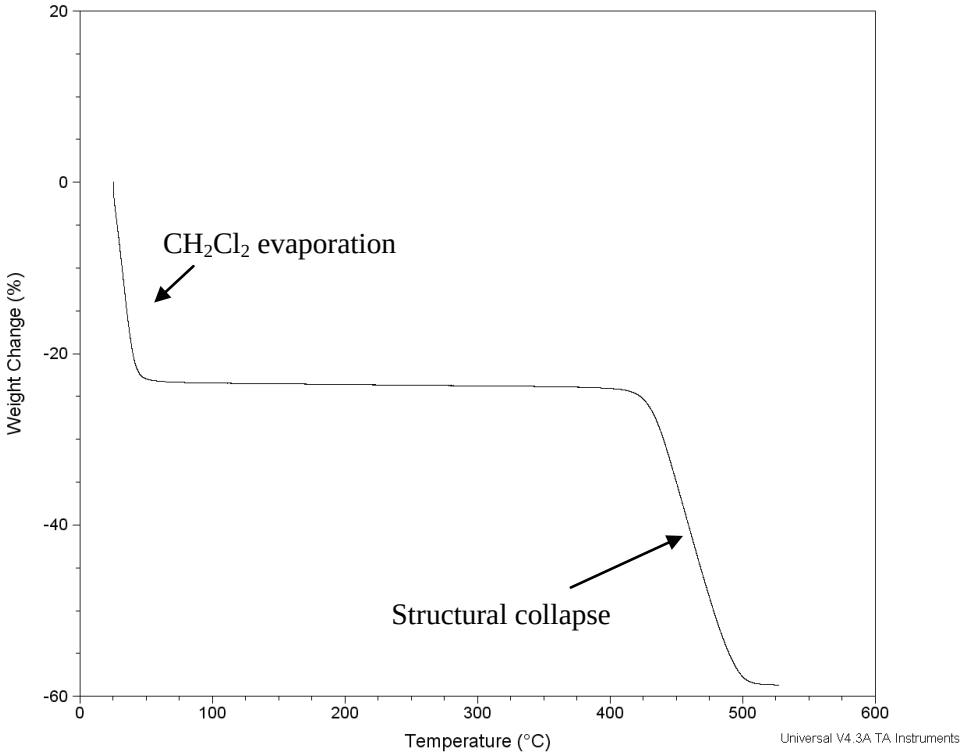

Figure 2.9. Thermal gravimetric analysis trace of UMCM-8 in minimal dichloromethane.

2.6 Conclusions

UMCM-8 proves that highly porous MCPs are obtainable from a mixture of linear ditopic linkers. The mixed-linker strategy employed to synthesize UMCM-8 provides similar stability to cubic MCPs such as MOF-5 while avoiding the interpenetration issues that plague IRMOF-8.

The mechanics of MCP formation in a mixed linker system are not fully understood, and may warrant further study.

2.7 Experimental Section/Supporting Information

Synthesis of UMCM-8 H_2BDC (0.460 g, 2.77 mmol) and H_2NDC (0.598 g, 2.77 mmol) were dissolved in 250 mL of DEF via sonication. $Zn(NO_3)_2 \cdot 6H_2O$ (4.25 g, 14.28 mmol) was added to the solution. The mixture was sonicated for 15 minutes then heated in an oven at 100° C for three days. After three days, the sample was cooled to room temperature, and the crystals were washed three times with DMF (250 mL). The crystals were then exchanged in dichloromethane three times over the course of three days. Vacuum activation at room temperature removed the solvent, yielding UMCM-8. The yield of the reaction, determined by the weight of dry UMCM-8 (1.13 g), is 48.0% based on H_2BDC.

Preparation of BDC-NDC screen Stock solutions of H_2BDC (0.0264 g, 0.159 mmol in 6 mL DEF), H_2NDC (0.0343 g, 0.159 mmol in 6 mL DEF), and $Zn(NO_3)_2 \cdot 6H_2O$ (0.2856 g, 0.960 mmol in 12 mL DEF) were prepared. The stock solutions were sonicated for 15 minutes. BDC and NDC stock solutions were combined in 1 mL Zn stock solution in quantities equal to the molar ratio of the linker (with sum of ten) multiplied by 100 μL. The samples were heated in an oven at 85° C, shaken after 15 minutes heat, then heated for 48 hours, when crystal formation was observed. After crystal formation was observed, the samples were cooled to room temperature, and the mother liquor was exchanged three times with DMF (2 mL). The samples were then exchanged in dichloromethane three times over the course of three days. Crystalline products remained in dichloromethane solvent.

Computer modeling Possible structures resulting from linear linkers were predicted by tiling the repeating unit derived from the coordination modes. Geometric structures were optimized

using the Forcite Plus module in Material Studio 5.5 from Accelerys. BET surface areas were predicted from the optimized geometric structures using PLATON v.14.[31]

X-ray diffraction Powder X-ray diffraction was performed on a Rigaku R-Axis Spider diffractometer equipped with an image plate detector and Cu Kα radiation operating in transmission mode. The sample was set at 45° in χ, rotated in φ and oscillated in ω to minimize preferred orientation.

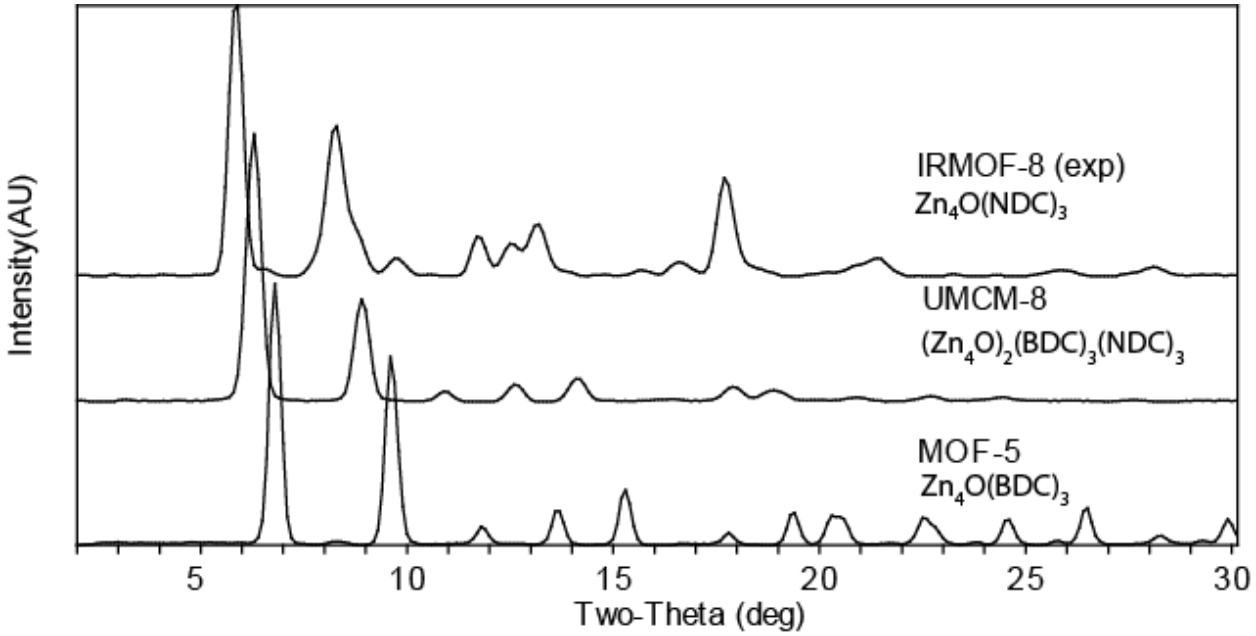

Figure 2.10. Powder X-ray diffraction patterns of IRMOF-8 (top), UMCM-8 (middle), and MOF-5 (bottom).

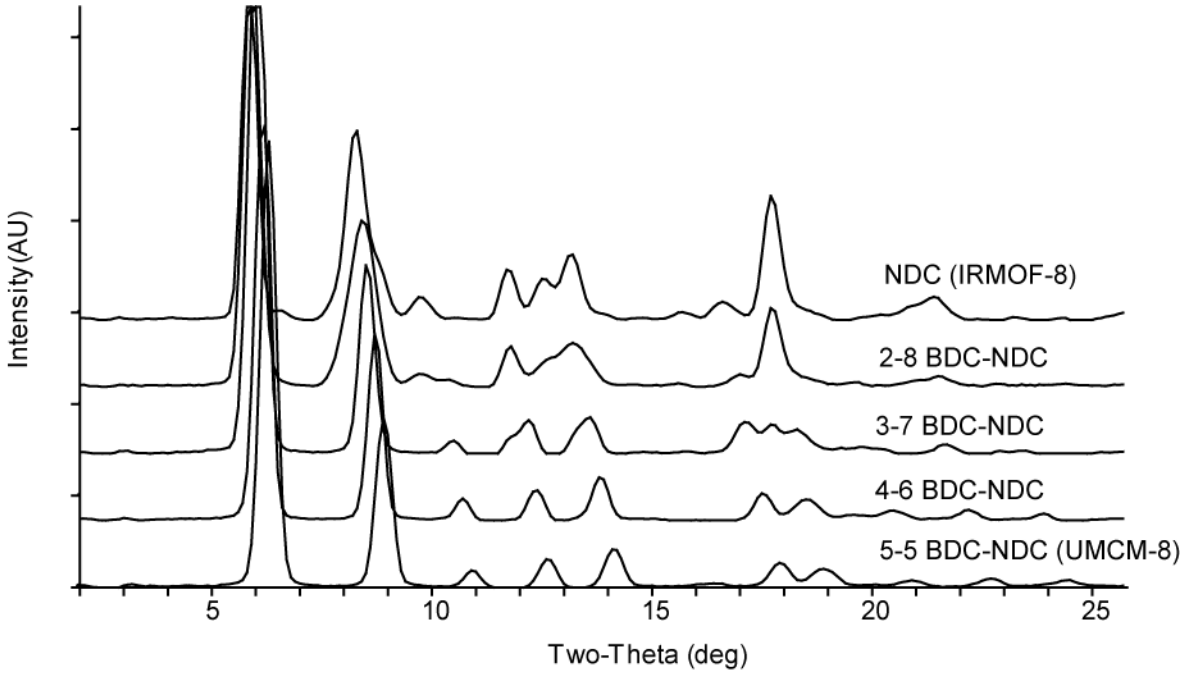

Figure 2.11. Powder X-ray diffraction patterns of BDC-NDC screen, from pure NDC (top) to a 5:5 BDC:NDC mol ratio (bottom).

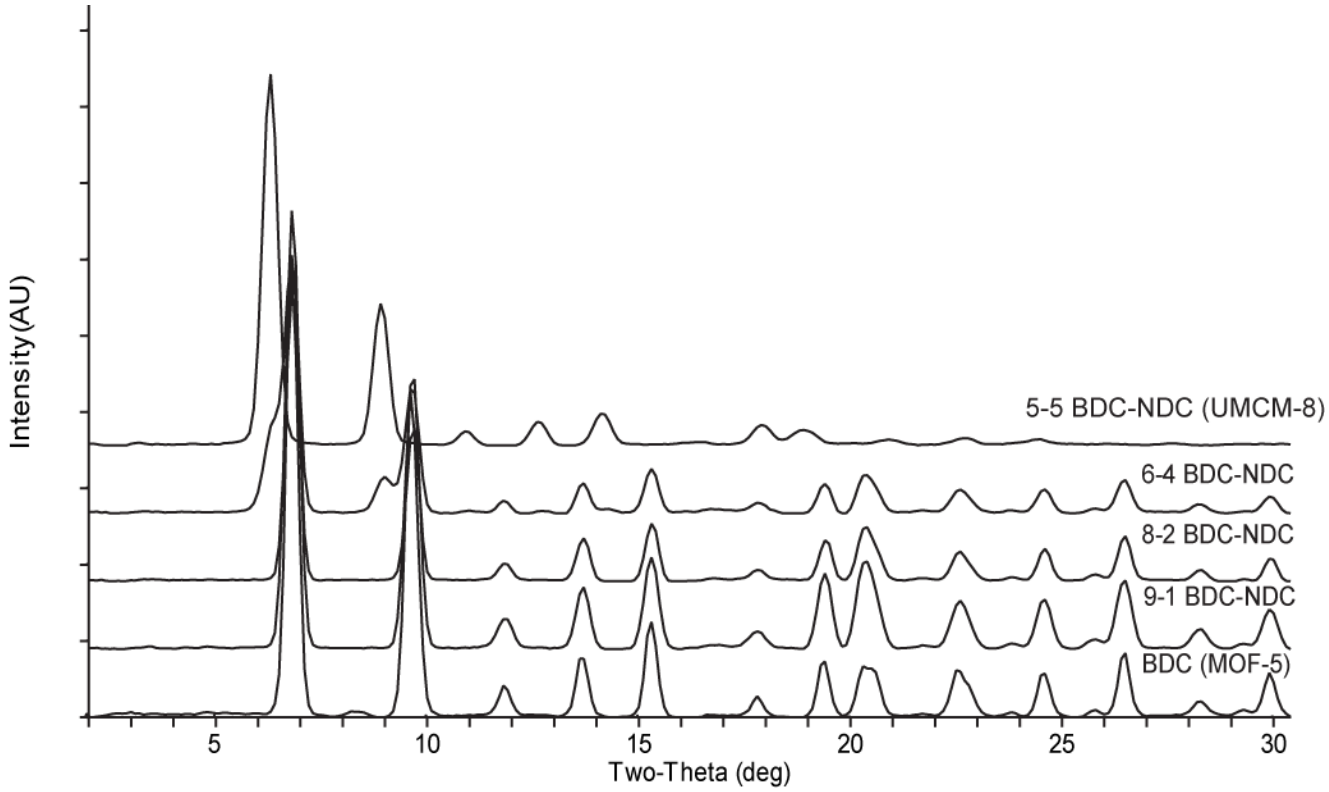

Figure 2.12. Powder X-ray diffraction patterns of BDC-NDC from 5:5 BDC:NDC mol ratio (top) to pure BDC (bottom).

Gas Sorption Measurements N_2 adsorption/desorption isotherms were measured volumetrically at 77 K N_2 adsorption/desorption isotherms were measured volumetrically at 77 K in the range $1.00 \times 10^{-5} \leq P/P_0 \leq 1.00$ with an Autosorb-1C outfitted with the micropore option by Quantachrome Instruments (Boynton Beach, Florida USA), running version 1.2 of the ASWin software package. Ultra-high purity He (99.999%, for void volume determination) and N_2 (99.999%) were purchased from Cryogenic Gasses and used as received. Samples were stored in CH_2Cl_2. UMCM-8 was dried under vacuum (< 0.1 millitorr) at room temperature. The resulting mass of dried material in the cell was ~30 mg.

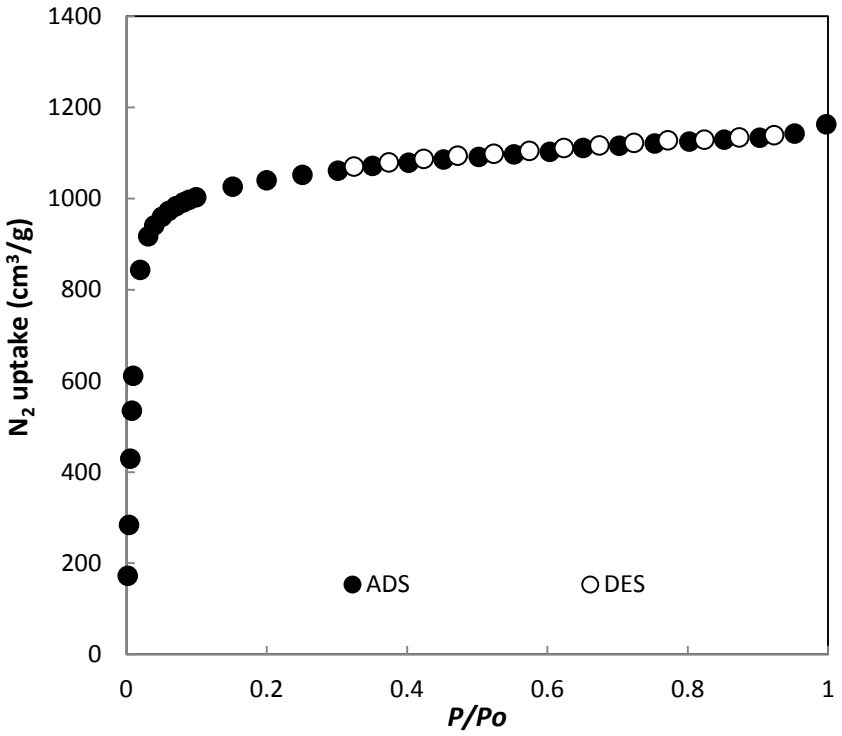

Figure 2.13. Nitrogen isotherm for UMCM-8 taken at 77 K.

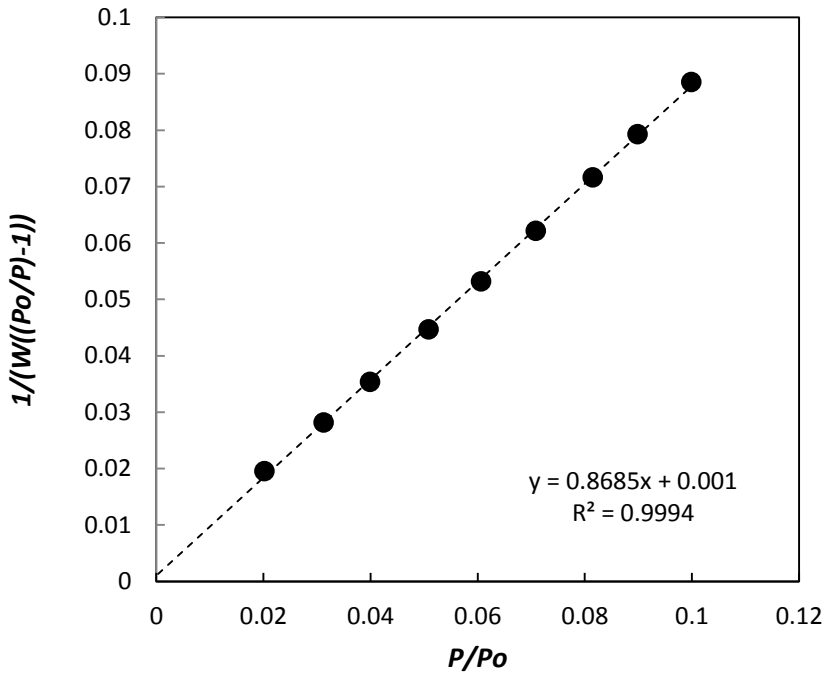

Figure 2.14. BET fit for the N2 adsorption isotherm of UMCM-8 (BET SA = 4005 m2/g). The relative pressure range ($0.02 \leq P/Po \leq 0.1$) for calculating the surface area satisfies the criteria for applying BET theory.[32]

^{1}H-NMR Studies of BDC-NDC screen Composition of linkers in MCPs was determined by ^{1}H-NMR spectroscopy. Approx. 10 mg dried crystals were decomposed in 1 M NaOD in D_2O solution. NMR spectra were obtained on a Varian MR 400 400 MHz spectrometer.

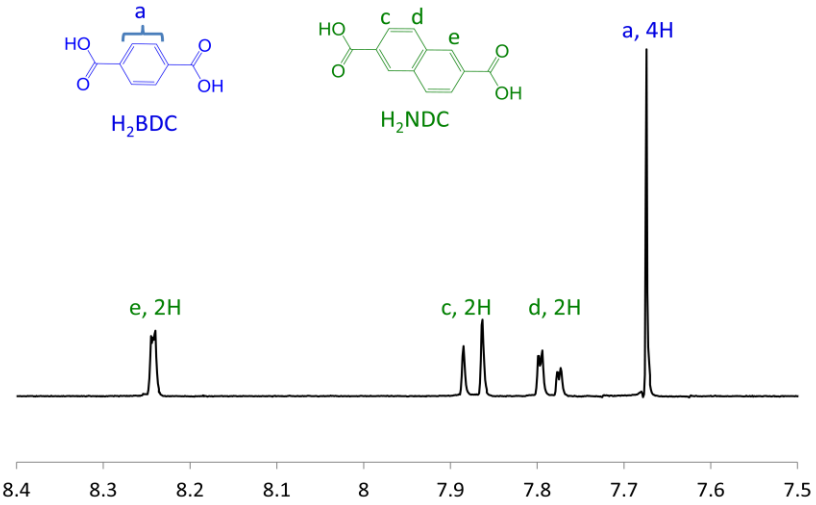

Figure 2.15. 1H-NMR spectrum after digesting UMCM-8 in 1 M NaOD . Integration of the BDC and NDC peaks yielded a BDC content of 45 mol %.

Chapter 3 - Mixed linker studies of H_2BDC, H_2NDC, and H_2BPDC and a highly porous MCP isostructural to UMCM-8

3.1 Introduction

Results of the previous chapter demonstrated the viability of combining H_2BDC and H_2NDC with Zn_4O clusters to synthesize a non-interpenetrated MCP with high surface area. Applying the principles used in the synthesis of UMCM-8 to other mixed-linker systems can potentially showcase the breadth of the synthetic strategy. Studies on based on UMCM-1 show longer linkers can be used to produce an MCP similar to existing MCPs, but with much higher surface area. Koh, et al. replaced H_2BDC with thieno[3,2-b]thiophene-2,5-dicarboxylate (H_2T_2DC) to produce UMCM-2, an MCP isostructural to UMCM-1 with over 5000 m^2/g BET surface area.[20] Furukawa, et al. increased the length of both linkers, using 4,4',4''-[benzene-1,3,5-triyl-tris(ethyne-2,1-diyl)]tribenzoate (H_3BTE) and biphenyl-4,4'-dicarboxylate (H_2BPDC) to produce MOF-205, an MCP with BET surface area of 6240 m^2/g.1 However, UMCM-1 and MOF-210 are not isostructrual. Scheme 1 shows the different linker combinations used to produce MCPs with linkers similar to those used to produce UMCM-1.

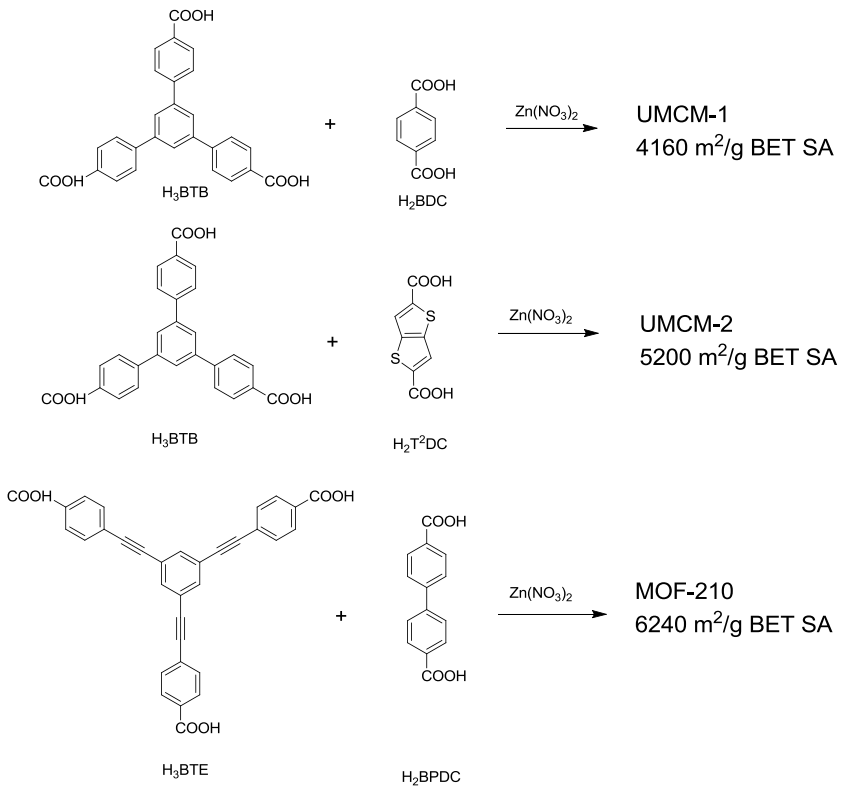

Figure 3.1. Increasing the length of the linkers in a mixed linker system can greatly increase the surface area of the resulting MCP.

On a similar note, replacing H_2BDC or H_2NDC with H_2BPDC under the conditions used to produce UMCM-8 may yield an MCP with greater surface area than UMCM-8 while maintaining UMCM-8's resistance to structural interpenetration. BPDC is known to react with Zn_4O clusters to yield doubly interpenetrated IRMOF-9 and non-interpenetrated IRMOF-10, an MCP isostructural to MOF-5 and IRMOF-8. IRMOF-9 possesses a BET surface area greater than IRMOF-8 (1904 m^2/g).[14]

3.2 Strategy

A three-linker screen composed of H_2BDC, H_2NDC, and H_2BPDC enables thorough exploration of the bonding patterns of linear linkers. While the results at equivalent mol percent concentrations of two linkers are known from UMCM-8 studies, and can thus be extrapolated upon to predict the properties of BDC-BPDC and NDC-BPDC mixtures, the presence of three

linkers in one solution can add potentially unforeseen complexities to MCP formation. A large screen enables the examination of a large number of differing linker-ratio concentrations. X-ray diffraction, nitrogen adsorption, and ^{1}H-NMR analyses of results will properly characterize any newly discovered MCPs.

3.3 Analysis of three-linker screen composed of H_2BDC, H_2NDC, and H_2BPDC

Due to solubility issues with H_2BPDC, the screen was run in a 2:1 volumetric solution of n-methylpyrrilidinone (NMP) to DEF. A mixture of three separate linkers could potentially yield one single MCP composed of three different linkers, one single MCP composed of two linkers, a mixture of MCPs composed of two linkers, or a mixture of MCPs composed of one linker. Figure 3.2 shows, at points where the results could be identified, most mixtures of the three linkers formed exactly one MCP. One new MCP powder pattern was consistently observed in the screen, and was called UMCM-9.

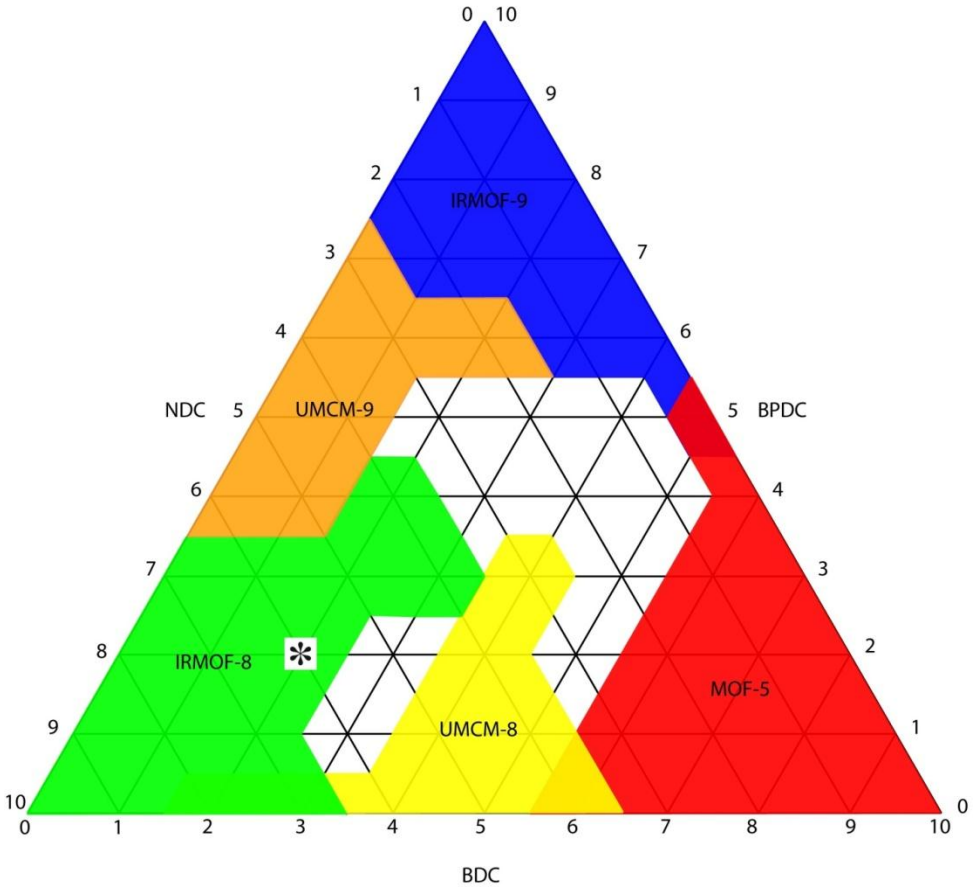

Figure 3.2. Three-linker diagram of BDC-NDC-BPDC screen. From a given point, follow the line downard to the left to obtain the BDC mol ratio, follow the line upward to the right to obtain the NDC mol ratio, and follow the line across to the right to obtain the BPDC mol ratio. Shaded areas represent ratios where known MCPs were obtained.

A mixture of MOF-5 and IRMOF-9 was observed at a 1:1 mol ratio of BDC and BPDC, as opposed to a new MCP isostructural to UMCM-8. Two apparent crystal morphologies were observed at equal concentrations of BDC and BPDC, but PXRD analysis showed one crystal morphology to be composed of IRMOF-9, a doubly interpenetrated cubic MCP composed of BPDC and Zn_4O clusters, and the other to be composed of a mixture of IRMOF-9 and MOF-5 (Figure 3.3).

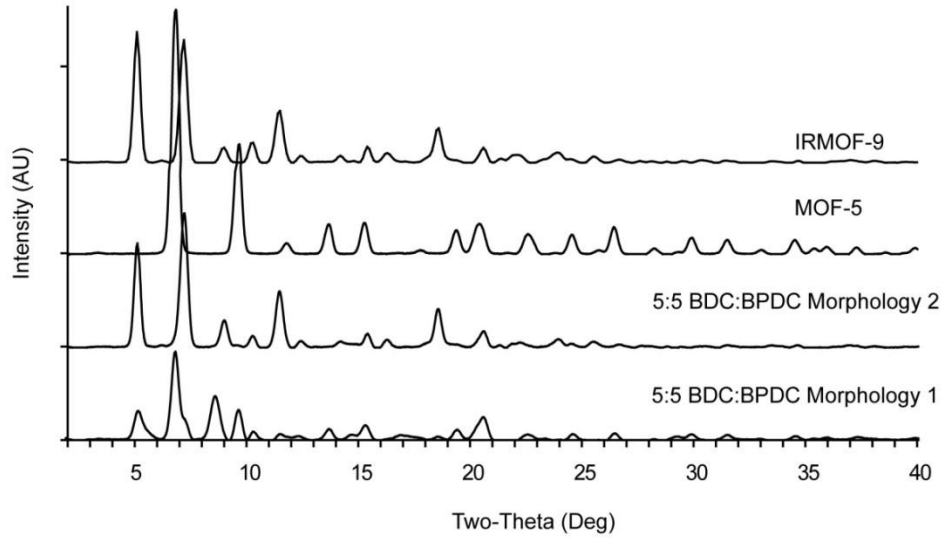

Figure 3.3. PXRD comparison between IRMOF-9 (top), MOF-5 (upper middle), and MCPs obtained from a 5:5 mol ratio of BDC and BPDC.

As Figure 3.3 demonstrates, the secondary morphology almost exactly matches the powder pattern of IRMOF-9. The powder pattern of the primary morphology matches most peaks with IRMOF 9, but also has peaks at 9.7°, 14.8°, 15.4° two-theta which closely match peaks observed in MOF-5's powder pattern. Since no MCP similar to UMCM-8 was observed when H_2BDC and H_2BPDC were mixed, it can be concluded that merely mixing linear linkers cannot guarantee the formation of a single, highly porous MCP. Further study could determine the presence of an upward limit to the difference in length between two linear linkers which can copolymerize to form a 2-linker MCP.

The blank areas on Figure 3.2 represent BDC-NDC-BPDC ratios in which no specific MCP could be identified. All blank ratios yielded one single MCP which displayed powder patterns similar to those displayed by cubic MOF-5 and IRMOF-8, and tetragonal UMCM-8 and UMCM-9. The locations of the peaks were shifted either to the right or to the left in comparison with powder patterns of previously known MCPs. It is quite likely that these crystals possess unique structures, but the high likelihood of linkers which do not directly contribute to the crystal

structure, as in the BDC-NDC screen, render single-crystal x-ray diffraction extremely difficult. The addition of a third linker to a mixed-linker system greatly increases the number of potential crystal structures, which rendered the modeling strategy used to address the BDC-NDC screen unviable.

The asterisk in Figure 3.2 located at a 2:6:2 BDC-NDC-BPDC mol ratio corresponds to a sample displaying intriguing characteristics. Powder x-ray diffraction of the sample matches very well with the predicted powder pattern of non-interpenetrated IRMOF-8 (Figure 3.4-a). Instead of the poor quality cube-like IRMOF-8 crystals (Figure 3.4-c), large, clear, cubic crystals (Figure 3.4-b) are formed. In all other IRMOF-8 producing mol ratios, the IRMOF-8 was of poor phase purity, similar to the IRMOF-8 obtained in the BDC-NDC screen in Chapter 2.

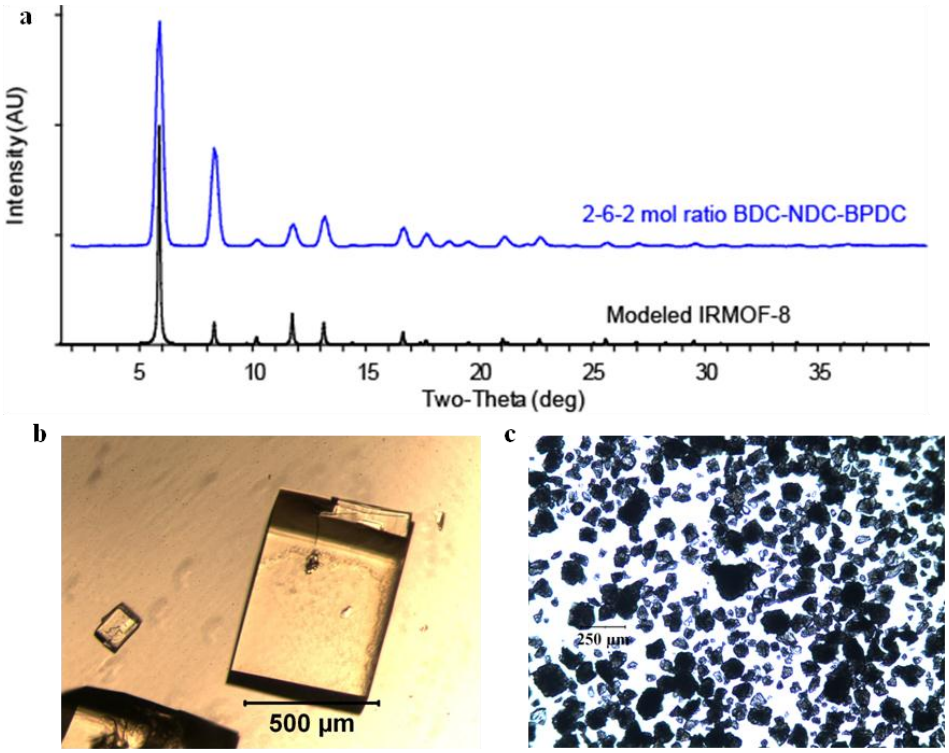

Figure 3.4. a. PXRD patterns of predicted non-interpenetrated IRMOF-8 (bottom) and sample obtained from 2-6-2 mol ratio of BDC, NDC and BPDC (top). b. Cubic crystals obtained at 2-6-2 mol ratio of BDC, NDC, and BPDC. c. Poor phase-purity IRMOF-8 obtained at other BDC-NDC-BPDC mol ratios.

A nitrogen adsorption isotherm of a 2:6:2 BDC-NDC-BPDC mol ratio gave a BET surface area of 4263 m^2/g, which closely matches the maximum available surface area of IRMOF-8.[17] It would appear that a specific mol ratio of three linkers can yield non-interpenetrated IRMOF-8, but single crystal x-ray diffraction failed to yield a solved crystal structure and ^{1}H-NMR of digested product in D_2O showed significant presence of BDC and BPDC in the product. Integration of key BDC and BPDC NMR peaks showed the IRMOF-8-like compound to be composed of 13 mol % BDC, 80 mol % NDC, and 7 mol % BPDC. Since the IRMOF-8-like compound is composed of 20% non-NDC linkers, we hypothesize that the sample is not pure IRMOF-8 and could potentially contain small quantities of MOF-5 and IRMOF-9. In addition, the inability of single-crystal diffraction to yield a crystal structure suggests that BDC and BPDC are interacting in unknown ways within the crystal lattice. BDC and BPDC could potentially be contributing to the crystal structure in a disorganized fashion, which is suggested by a lack of PXRD peaks which do not match with the predicted PXRD pattern of non-interpenetrated IRMOF-8. However, why the specific 2-6-2 mol ratio of BDC, NDC, and BPDC forms the highly porous IRMOF-8-like substance and not similar mol ratios of linkers is unknown and difficult to determine experimentally.

3.4 Discovery of UMCM-9, an MCP isostructural to UMCM-8 displaying remarkable surface area

UMCM-9 was found to have a tetragonal unit cell isostructural to UMCM-8 (Figure 3.5-a) resulting from NDC and BPDC ligands coordinated to Zn_4O clusters in a facial arrangement (Figure 3.5-b).

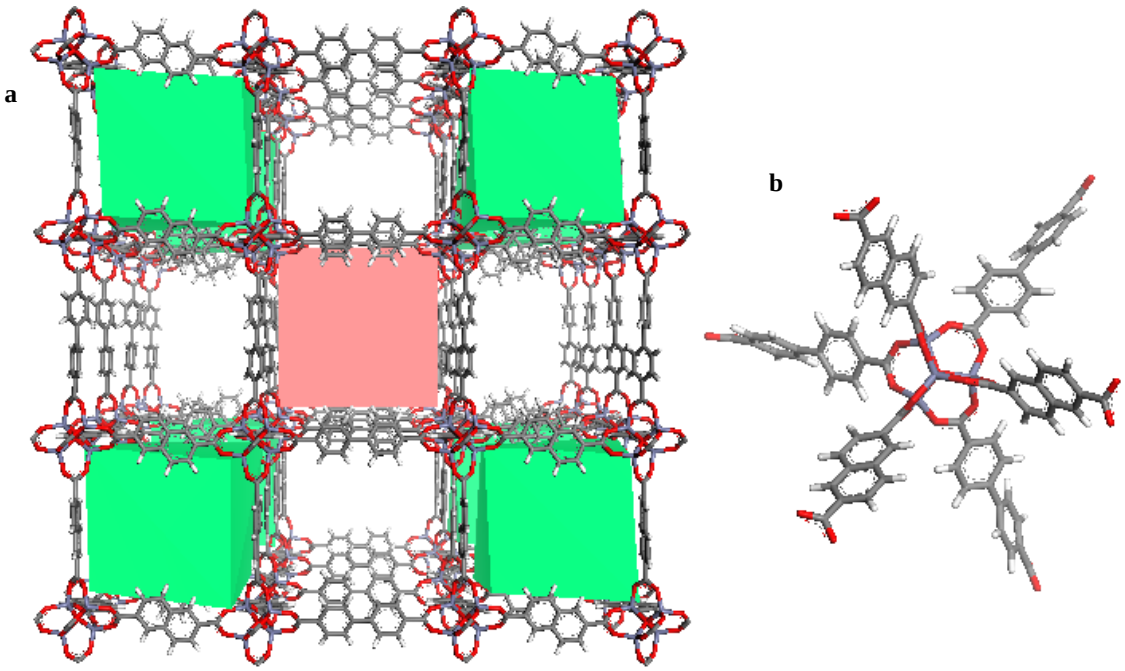

Figure 3.5. a. Unit cell structure of UMCM-9, composed of cubic NDC and BPDC cages connected at the corner. b. Facially arranged $Zn_4O(NDC)_3(BPDC)_3$ UMCM-9 cluster.

Like UMCM-8, UMCM-9's unit cell is composed of one cubic BPDC cage, 8 cubic NDC cages, 6 tetragonal cages composed of 8 BPDC and 4 NDC, and 8 tetragonal cages composed of 4 BPDC and 8 NDC.

As attempts to use single-crystal x-ray diffraction to solve the crystal structure of UMCM-9 failed due to consistently poor diffraction of the crystals, the UMCM-9 unit cell was modeled. Pawley refinements of the modeled structure were compared to PXRD patterns obtained from UMCM-9 samples. A Pawley refinement of the powder x-ray pattern of the modeled structure closely matches the experimental results obtained from a 1:1 mol ratio of H_2NDC and H_2BPDC (Figure 3.6).

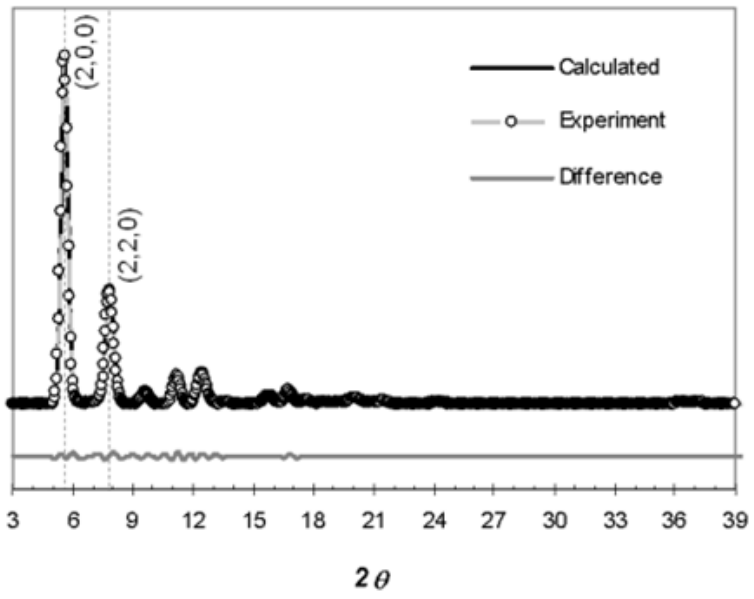

Figure 3.6. Overlay of Pawley refinement results from PXRD patterns of simulated fac-$(Zn_4O)(NDC)_3(BPDC)_3$and experimental PXRD patterns of UMCM-9.

Analysis of the simulated UMCM-9 structure using PLATON predicted a BET surface area of 4900 m^2/g. However, a nitrogen adsorption isotherm taken after traditional evacuation of dichloromethane solvent under vacuum yielded a BET surface area of only 1330 m^2/g. PXRD patterns of UMCM-9 before and after dichloromethane evacuation (Figure 3.7) suggest a structural change in the crystal after evacuation, which is indicative of structural collapse.

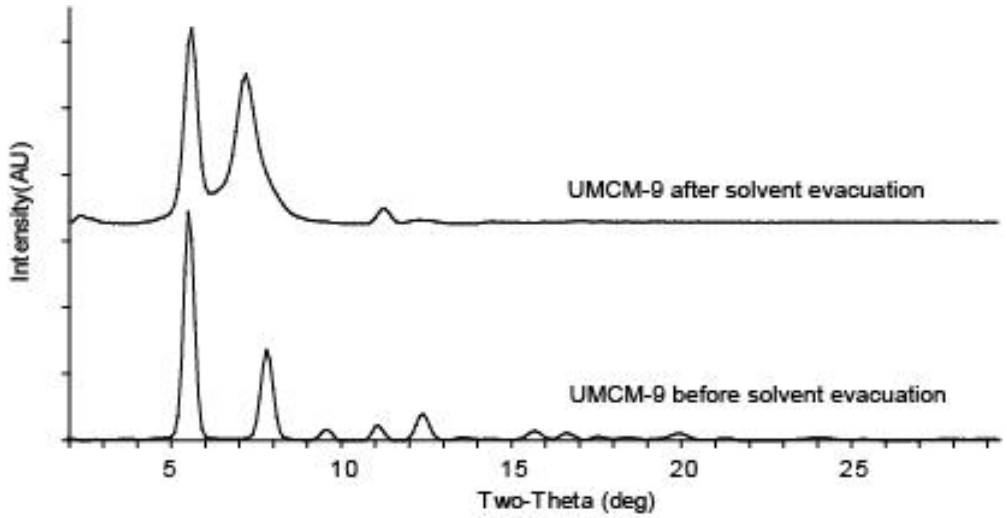

Figure 3.7. PXRD pattern of UMCM-9 before evacuation of dichloromethane solvent (bottom) and UMCM-9 after evacuation of dichloromethane solvent (top).

Although the peaks at 5.5° and 11° two-theta are unchanged after evacuation, the smaller peak at 7.8° two-theta shifts significantly, suggesting significant structural changes in the tetragonal cage.

Alternate methods of solvent removal exist which can reduce the likelihood of structural collapse during activation of MCPs. Instead of the traditional activation method, in which the mother liquor (usually DMF or DEF) is exchanged with a more volatile solvent such as dichloromethane or THF, which is then evacuated under vacuum, Nelson, et. al. proposed activation via supercritical CO_2 as a method to greatly increase accessible surface area.[33] It was hypothesized that, since CO_2 at temperatures and pressures above the critical point lacks surface tension, capillary forces would prevent the structural collapse of the MCP.

A nitrogen adsorption isotherm of UMCM-9 after supercritical CO_2 activation showed activated UMCM-9 to have a BET surface area of 4969 m^2/g. Had UMCM-9 suffered from interpenetration and not structural collapse, CO_2 activation of UMCM-9 should not have yielded such a dramatic increase in accessible surface area.

Thermal gravimetric analysis of UMCM-9 showed two primary weight-loss steps – solvent evaporation finishing at approximately 50° C, and structural collapse between 400-500° C (Figure 3.8). Structural collapse represented a 42% weight loss. Like UMCM-8, no weight loss steps were observed between solvent evaporation and structural collapse. If UMCM-8's pores were too large to prevent complete evaporation of dichloromethane solvent, UMCM-9's larger framework would be expected to yield similar results. UMCM-9 has slightly lower thermal stability than UMCM-8, but is still stable up to 400°C. Thermal stability of UMCM-9 similar to MOF-5,[30] along with the BET surface area obtained after supercritical CO_2 activation, demonstrates that UMCM-9 possesses the structural integrity afforded by cubic MCPs while avoiding interpenetration issues which plague IRMOF-8 and IRMOF-9.

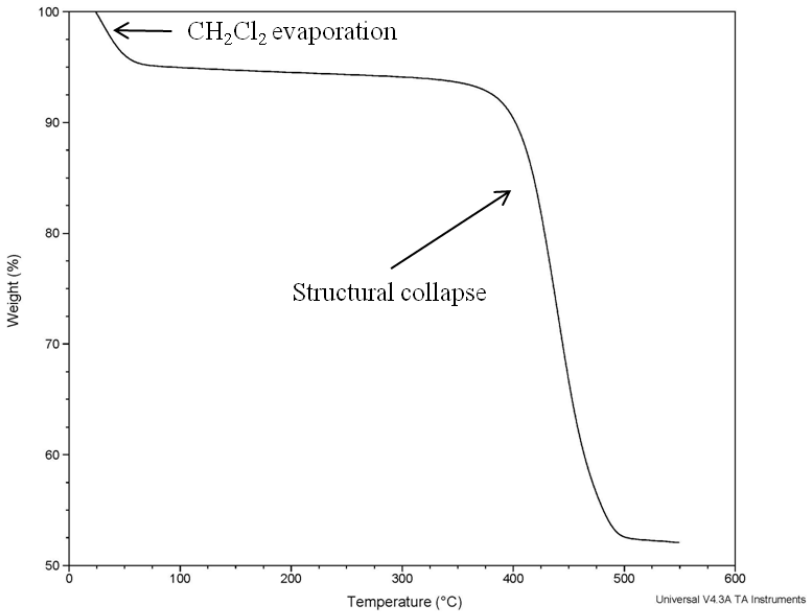

Figure 3.8. TGA trace of UMCM-9 in minimal dichloromethane.

3.5 Conclusions

A screen composed of three linear linkers H_2BDC, H_2NDC, and H_2BPDC demonstrated the strengths and limitations of multiple linker screens. Equal mol ratios of H_2NDC and H_2BPDC were combined to yield highly porous, noninterpenetrated UMCM-9. Structural stability concerns mandate CO_2 activation to achieve high surface areas for UMCM-9. Some combinations of linear linkers, such as a combination of H_2BDC and H_2BPDC, fail to copolymerize into a new MCP. A three-linker screen can showcase peculiar and unexplained chemistry as demonstrated by the formation of a structure very similar to IRMOF-8 at one specific combination of linkers and displaying remarkable porosity, but containing significant quantities of BDC and BPDC.

3.6 Experimental Section/Supporting Information

Synthesis of UMCM-9 H_2NDC (28.7 mg, 0.132 mmol) and H_2BPDC (35.6 mg, 0.147 mmol) were dissolved in a mixture of 6.7 mL of DEF and 13.3 mL of *N*-methyl pyrrolidone. $Zn(NO_3)_2 \cdot 6H_2O$ (0.238 g, 0.800 mmol) was added to the solution. The mixture was sonicated for 15 min and heated to 85 °C. After 4 days, crystals of a single phase were obtained. After cooling to room temperature the product was isolated by decanting the mother liquor and washing with DMF (3 × 20 mL). The resulting solid was then immersed in 20 mL CH_2Cl_2 for 2 days, during which time the CH_2Cl_2 was replaced three times then sample was stored in CH_2Cl_2. The yield of the reaction, determined from the weight of the solvent-free material (57.9 mg), is 41.8 % based on H_2NDC.

Supercritical CO_2 Activation of UMCM-9 Activation was performed with a Jasco PU-1580-CO_2 delivery pump equipped with a back pressure regulator (Jasco BP-1580-81). The CH_2Cl_2-

soaked sample (0.1 g) was placed a metal column and CH_2Cl_2 was exchanged with liquid CO_2 at 100 bar; the liquid CO_2–charged column was heated at 35 °C for 30 min. CO_2 was vented over 30 minutes via the back pressure regulator to obtain the activated sample.

Preparation of Three-Linker Screen

Stock solutions of H_2BDC (0.1055 g, 0.635 mmol in a mixture of 16 mL NMP and 8 mL DEF), H_2NDC (0.1372 g, 0.635 mmol in a mixture of 16 mL NMP and 8 mL DEF), H_2BPDC (0.1715 g, 0.635 mmol in a mixture of 16 mL NMP and 8 mL DEF), and $Zn(NO_3)_2 \cdot 6H_2O$ (1.714 g, 5.76 mmol in a mixture of 48 mL NMP and 24 mL DEF) were prepared and sonicated for 15 minutes. The screen was prepared by adding to one mL Zn stock solution each ratio of BDC, NDC, and BPDC adding up to 1 mL. For example, the 3:3:4 BDC:NDC:BPDC sample was prepared by adding 300 μL BDC stock solution, 300 μL NDC stock solution, and 400 μL BPDC stock solution to 1 mL Zn stock solution. All samples were heated to 85 °C, shaken after 15 minutes heat, then left in the oven. After 4 days, crystal formation was observed. All samples were cooled to room temperature, and products were isolated by decanting the mother liquor and washing with DMF (3 × 2 mL per sample). The resulting solids were each immersed in 2 mL CH_2Cl_2 for three days, during which time the CH_2Cl_2 was replaced with fresh CH_2Cl_2 three times.

Preparation of IRMOF-8-like sample

H_2BDC (0.0088 g, 0.0529 mmol), H_2NDC (0.0343 g, 0.1587 mmol), and H_2BPDC (0.0357 g, 0.0529 mmol) were dissolved in a mixture of 12 mL NMP and 8 mL DEF. $Zn(NO_3)_2 \cdot 6H_2O$ (0.2380 g, 0.800 mmol) was added to the solution, which was then sonicated for 15 minutes, then heated to 85 °C. The sample was shaken after 15 minutes heating, then left in the oven. After 4 days, crystals of a single phase were obtained. After cooling to room temperature the product

was isolated by decanting the mother liquor and washing with DMF (3 × 20 mL). The resulting solid was then immersed in 20 mL CH_2Cl_2 for 2 days, during which time the CH_2Cl_2 was replaced three times then sample was stored in CH_2Cl_2.

X-ray diffraction Powder X-ray diffraction was performed on a Rigaku R-Axis Spider diffractometer equipped with an image plate detector and Cu Kα radiation operating in transmission mode. The sample was set at 45° in χ, rotated in φ and oscillated in ω to minimize preferred orientation.

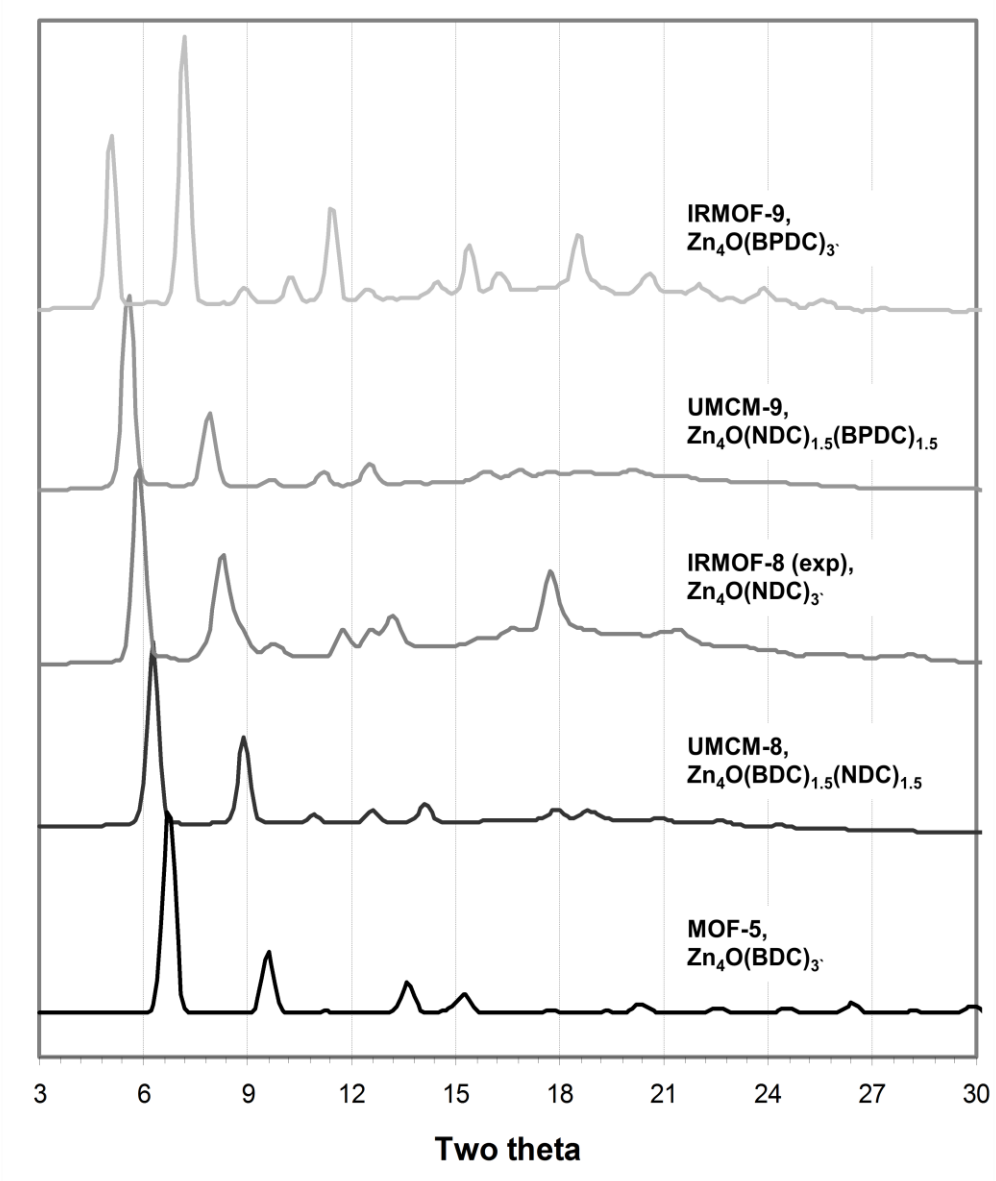

Figure 3.9. PXRD patterns of IRMOF-9, UMCM-9, IRMOF-8, UMCM-8, and MOF-5 (top to bottom).

Gas Sorption Measurements N_2 adsorption/desorption isotherms were measured volumetrically at 77 K N_2 adsorption/desorption isotherms were measured volumetrically at 77 K in the range $1.00 \times 10^{-5} \leq P/P_0 \leq 1.00$ with an Autosorb-1C outfitted with the micropore option by Quantachrome Instruments (Boynton Beach, Florida USA), running version 1.2 of the ASWin software package. Ultra-high purity He (99.999%, for void volume determination) and N_2 (99.999%) were purchased from Cryogenic Gasses and used as received. Samples were stored in

CH_2Cl_2. Samples were dried under vacuum (< 0.1 millitorr) at room temperature. The resulting mass of dried material in the cell was ~30 mg.

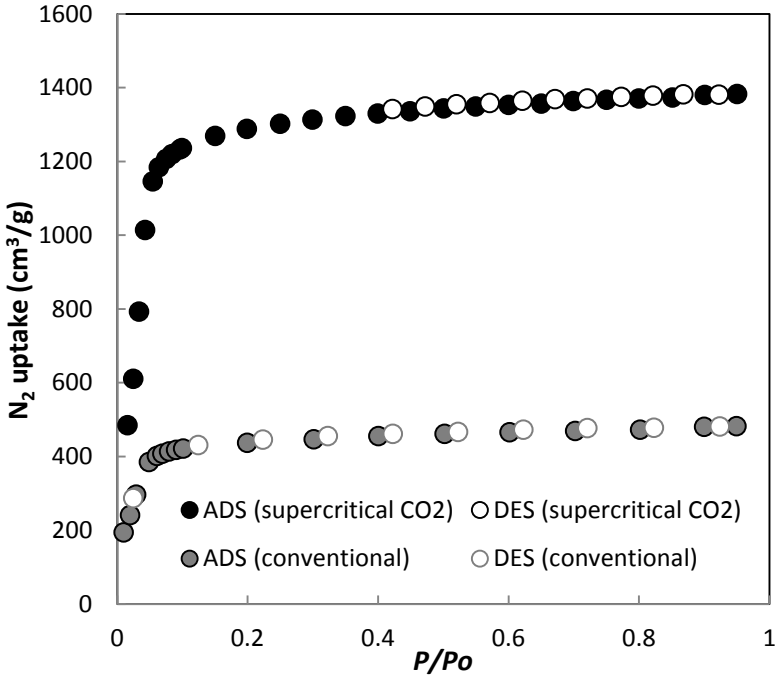

Figure 3.10. Nitrogen adsorption isotherms taken at 77 K for UMCM 9 after conventional solvent evacuation (black) and supercritical CO_2 activation (gray).

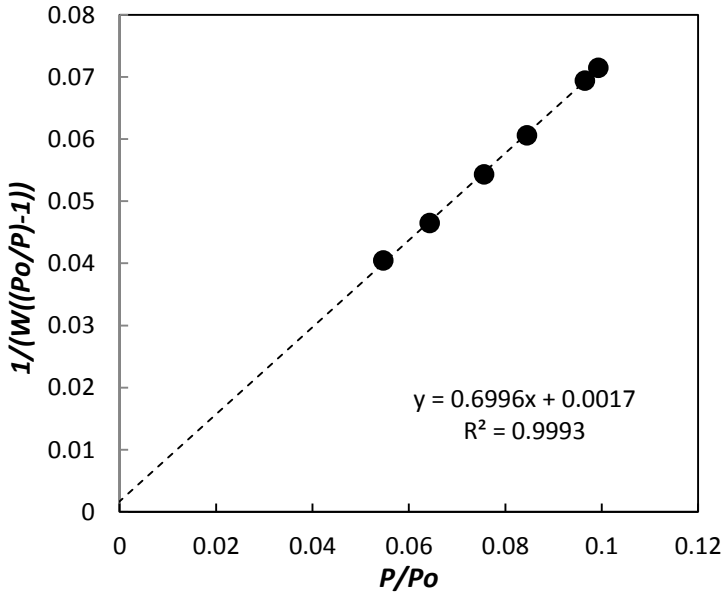

Figure 3.11. BET fit for the N2 adsorption isotherm of UMCM-9 (BET SA = 4969 m2/g). The relative pressure range ($0.05 \leq P/Po \leq 0.1$) for calculating the surface area satisfies the criteria for applying BET theory.[23]

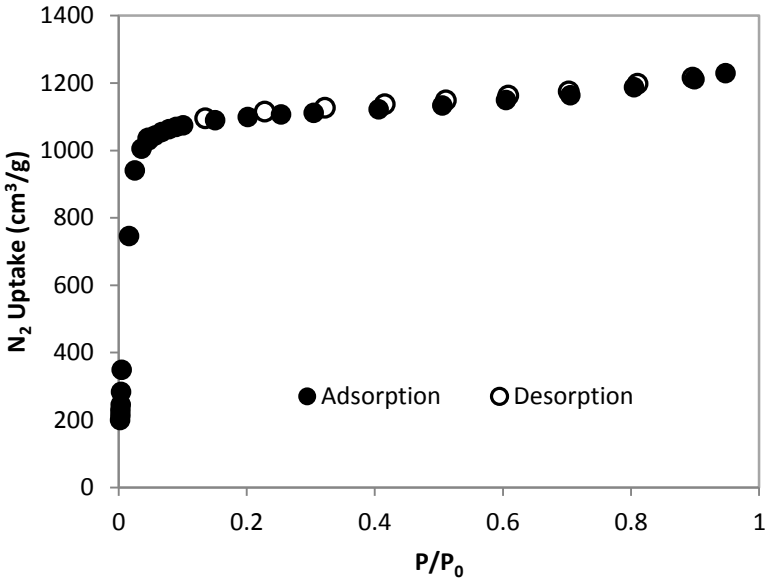

Figure 3.12. Nitrogen adsorption isotherm taken at 77 K of sample obtained from a 2:6:2 BDC-NDC-BPDC mol ratio.

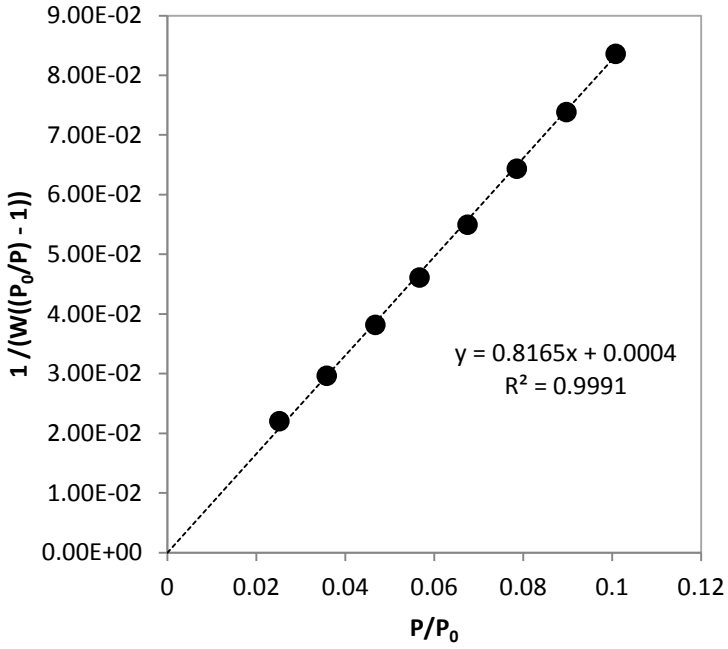

Figure 3.13. BET fit for the N2 adsorption isotherm of sample obtained from a 2:6:2 BDC-NDC-BPDC mol ratio (BET SA = 4263 m^2/g). The relative pressure range ($0.05 \leq P/Po \leq 0.1$) for calculating the surface area satisfies the criteria for applying BET theory.[23]

^{1}H-NMR Studies of UMCM-9 and BDC-NDC-BPDC screen Composition of linkers in MCPs was determined by ^{1}H-NMR spectroscopy. Approx. 10 mg dried crystals were decomposed in 1 M NaOD in D_2O solution. NMR spectra were obtained on a Varian MR 400 400 MHz spectrometer.

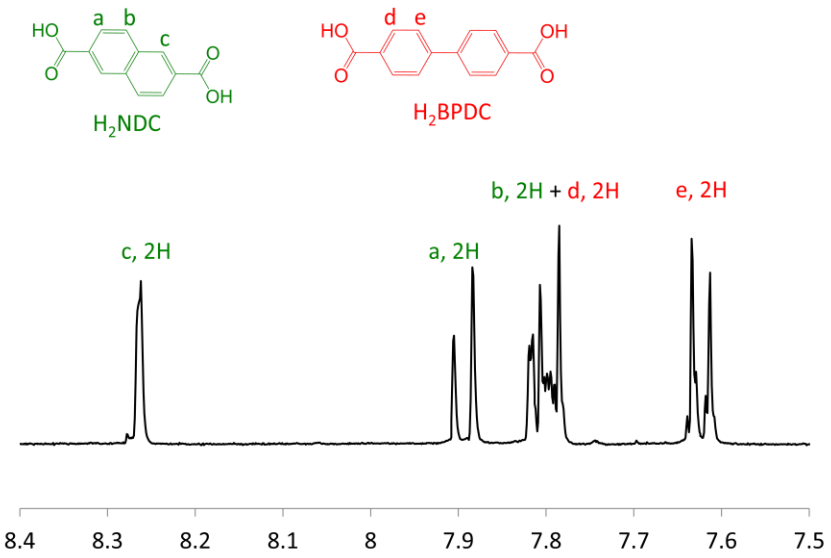

Figure 3.14. ^{1}H-NMR spectrum of UMCM-9 after digesting in 4 wt% NaOD solution. From the integration values of peaks, the empirical formula is estimated as $Zn_4O(NDC)_{1.32}(BPDC)_{1.68}$.

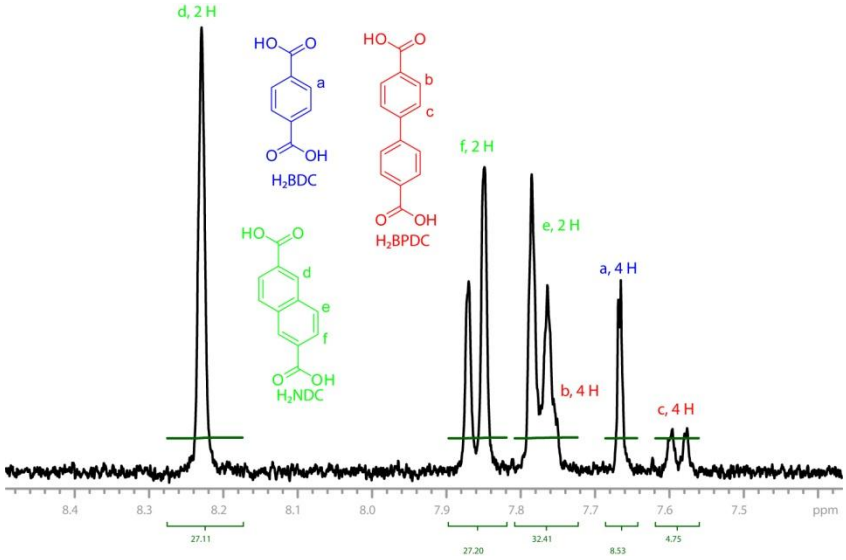

Figure 3.15. 1H-NMR spectrum of sample obtained from a 2-6-2 BDC-NDC-BPDC mol ratio after digesting in 4 wt% NaOD solution. From the integration values of the peaks, the sample contains 13 mol % BDC, 80 mol % NDC, and 7 mol % BPDC.

References

[1] Furukawa, H.; Ko, N.; Go, Y. B.; Aratani, N.; Choi, S. B.; Choi, E.; Yazaydin, A. O.; Snurr, R. Q.; O'Keeffe, M.; Kim, J.; Yaghi, O. M. *Science* **2010**, *329*, 424-428

[2] Murray, L. J.; Dinca, M.; Long, J. R. *Chem. Soc. Rev.* **2009**, *38*, 1294-1314.

[3] Lee, J.; Farha, O. K.; Roberts, J.; Scheidt, K. A.; Nguyen, S. T.; Hupp, J. T., *Chem Soc Rev* **2009,** *38* (5), 1450-1459.

[4] Keskin, S.; van Heest, T. M.; Sholl, D. S., *Chemsuschem* **2010,** *3* (8), 879-891.

[5] Cychosz, K. A.; Wong-Foy, A. G.; Matzger, A. J., *J Am Chem Soc* **2009,** *131* (40), 14538-14543..

[6] Yaghi, O. M.; O'Keeffe, M.; Ockwig, N. W.; Chae, H. K.; Eddaoudi, M.; Kim, J., *Nature* **2003,** *423* (6941), 705-714.

[7] Rosi, N. L.; Eckert, J.; Eddaoudi, M.; Vodak, D. T.; Kim, J.; O'Keeffe, M.; Yaghi, O. M., *Science* **2003,** *300* (5622), 1127-1129.

[8] Chae, H. K.; Siberio-Perez, D. Y.; Kim, J.; Go, Y.; Eddaoudi, M.; Matzger, A. J.; O'Keeffe, M.; Yaghi, O. M., *Nature* **2004,** *427* (6974), 523-527.

[9] Chui, S. S. Y.; Lo, S. M. F.; Charmant, J. P. H.; Orpen, A. G.; Williams, I. D., *Science* **1999,** *283* (5405), 1148-1150.

[10] Sing, K. S. W.; Everett, D. H.; Haul, R. A. W.; Moscou, L.; Pierotti, R. A.; Rouquerol, J.; Siemieniewska, T., *Pure and Applied Chemistry* **1985,** *57* (4), 603-619.

[11] S. Brunauer, P. H. Emmett and E. Teller, *J. Am. Chem. Soc.*, 1938, **60**, 309.

[12] Batten, S. R.; Robson, R., *Angew Chem Int Edit* **1998,** *37* (11), 1460-1494.

[13] Reineke, T. M.; Eddaoudi, M.; Moler, D.; O'Keeffe, M.; Yaghi, O. M., *J Am Chem Soc* **2000,** *122* (19), 4843-4844.

[14] Eddaoudi, M.; Kim, J.; Rosi, N.; Vodak, D.; Wachter, J.; O'Keeffe, M.; Yaghi, O. M., *Science* **2002,** *295* (5554), 469-472.

[15] Yuan, D. Q.; Zhao, D.; Sun, D. F.; Zhou, H. C., *Angew Chem Int Edit* **2010,** *49* (31), 5357-5361.

[16] Wong-Foy, A. G.; Lebel, O.; Matzger, A. J., *J Am Chem Soc* **2007,** *129* (51), 15740-15741.

[17] Schnobrich, J. K.; Koh, K.; Sura, K. N.; Matzger, A. J. *Langmuir* **2010**, *26*, 5808.

[18] Grzesiak, A. L.; Uribe, F. J.; Ockwig, N. W.; Yaghi, O. M.; Matzger, A. J., *Angew Chem Int Edit* **2006,** *45* (16), 2553-2556.

[19]Koh, K.; Wong-Foy, A. G.; Matzger, A. J., *Angew Chem Int Edit* **2008,** *47* (4), 677-680.

[20] Koh, K.; Wong-Foy, A. G.; Matzger, A. J., *J Am Chem Soc* **2009,** *131* (12), 4184-4185.

[21] Park, T. H.; Koh, K.; Wong-Foy, A. G.; Matzger, A. J., *Crystal Growth & Design* **2011,** *11* (6), 2059-2063.

[22] Rowsell, J. L. C.; Yaghi, O. M., *J Am Chem Soc* **2006,** *128* (4), 1304-1315.

[23] Walton, K. S.; Snurr, R. Q., *J Am Chem Soc* **2007,** *129* (27), 8552-8556.

[24] Rowsell, J. L. C.; Millward, A. R.; Park, K. S.; Yaghi, O. M. **2004**, *126*, 5666-5667.

[25] See supporting Information for powder patterns.

[26] Koh, K.; Wong-Foy, A. G.; Matzger, A. J., *Chem Commun* **2009,** (41), 6162-6164.

[27] For detailed explanation of NMR methodology, see Supporting Information

[28] For an explanation of computational methods, see Supporting Information

[29] For an explanation of surface area studies, see Supporting Information.

[30] Liu, Y. Y.; Ng, Z. F.; Khan, E. A.; Jeong, H. K.; Ching, C. B.; Lai, Z. P., *Microporous and Mesoporous Materials* **2009,** *118* (1-3), 296-301.

[31] Spek, A. L. *J Appl. Cryst.* **2003,** *36,* 7-13.

[32] Walton, K. S.; Snurr, R. Q. **2007**, *129*, 8552-8556.

[33] Nelson, A. P.; Farha, O. K.; Mulfort, K. L.; Hupp, J. T., *J Am Chem Soc* **2009,** *131* (2), 458-460.